SECONDARY CHARGED PARTICLE EMISSIONS INDUCED BY LOW-ENERGY ION IMPACT ON NON-METALLIC SURFACES

Kazumoto HOSAKA

Submitted as Partial Fulfillment
of the Requirements of
DOCTOR OF SCIENCE

at

The Graduate University for Advanced Studies
November 1997

Summary

It is well known that the interactions of energetic particles with solid surfaces lead to the emission of particles such as electrons and target atoms / ions from the target surface. This is usually referred to as the secondary particle emissions. One of the fundamental observations of this phenomenon is the measurement of the secondary particle emission yield, γ, defined as the average number of particles emitted per the incoming particle. There are a lot of experimental as well as theoretical studies on the secondary electron emission yields induced by ion impact on the *metal surfaces*. Therefore, the relevant mechanisms have been understood reasonably well. However, investigations on the secondary ion emission yields have still been limited.

Furthermore, only a few attempts have been made so far in understanding phenomena under ion impact on the *non-metallic surfaces* though alkali-halides have been investigated in some details. Therefore, we do not have sufficient understanding in the interaction mechanisms between ions and non-metallic surfaces.

The purpose of the present study is to reveal any difference in the interactions of ions with metal and non-metallic surfaces. Such studies are of great importance not only in basic physics but also in applied fields such as very-large-scale-integrated-circuits (VLSI) technology, fusion plasmas, surface analysis etc.

In the present study, the secondary electron emission yields, γ^-, and the secondary positive ion emission yields, γ^+, from some non-metallic surfaces induced by low energy ion (0.3～100 keV H^+, 2.5 keV H_2^+ and 2.5～150 keV Ar^+) impact have been measured using a cylindrical double-wall cup under an ultra high vacuum chamber ($\sim 10^{-11}$ Torr) pumped down with the combination of a turbo molecular pump, an ion pump and a titanium sublimation pump with a liquid nitrogen trap. In order to clean the target surfaces they were sputtered with argon ions and also heated with a ceramic heater placed behind the target. An Auger electron spectrometer has been used in order to check the surface cleanness.

It has been found that the observed γ^- from the non-metallic surfaces is proportional to the electronic stopping power over the collision energy range investigated. It is noted that similar relations are well known in metal targets. However, the proportional coefficients in γ^- observed in the non metallic targets are found to be 2-3 times larger than those for metal targets. These results agree with tendencies for oxygen-covered metal surfaces observed in the present experiment which show that γ^- increases as the oxygen coverage increases. We have also observed, for the first time, an interesting phenomenon where the observed γ^- in $SrCeO_3$ target strongly depends on the incident ion beam flux and becomes zero above a critical ion flux.

Similarly, we have found that the observed γ^+, which has been found to be independent of the incident ion flux investigated, is larger than the results calculated with the TRIM code. It has been found from TRIM code calculations, however, that a significant part of the observed γ^+ in proton and hydrogen molecular ion impact are due to the secondary electrons emitted from the wall of the inner cup under impact of the neutral hydrogen atoms backscattered from the target surfaces. Nevertheless, the observed γ^+ from non-metallic targets under argon ion impact is far large, compared with the calculated results. Then it has been found that γ^+ induced by argon ion impact on $SrCeO_3$ is proportional not to the nuclear stopping power but to the electronic stopping power. This result shows that a greater part of these secondary positive ions are not emitted through physical sputtering. The observed γ^+ in 2.5 keV argon ion impact seems to be in reasonable agreement with that extrapolated from the data available which is believed to be due to the Coulomb explosion on the non-metallic surfaces.

Furthermore, in order to identify the mass and energy of the secondary positive ions emitted from targets, two different techniques have been used: One was a collector method using graphite and beryllium sheets which were analyzed with Rutherford backscattering technique using 1.8 MeV helium ions. Another was the mass and energy analysis with a quadrupole mass spectrometer attached with

four meshes, to which the retarding voltage was applied for kinetic energy selection.

Both experiments confirm that target elements are emitted as ions (as well as neutrals) by the incident ion impact. Furthermore, the second experiment shows that these emitted ions have large kinetic energy, comparable to the incident ion energy. Such large kinetic energy can be qualitatively understood to be provided probably by the electrostatic potential caused by local charge-accumulation of the incident ions on the non-metallic surfaces due to their high resistivities. This phenomenon can also explain how the observed γ^- depends on the incident ion beam flux because some fractions of the electrons produced in the target are not able to overcome the Coulomb barrier generated by accumulation of the incident ion charge and can not be liberated into vacuum.

It is concluded from the present work that the key mechanisms responsible in the secondary particle emissions from the non-metallic surfaces are very different from those in metal targets induced by the energetic ion impact.

Contents

Chapter 1 Introduction

The emission of secondary particles and the backscattering of the projectile particles from the solid surfaces in the interactions between energetic particles and solids are the well-known phenomena. These secondary particles consist of sputtered atoms, molecules and ions, and secondary electrons. Photons are also one of the secondary particles, which are not discussed in the present study. One of the fundamental quantities is the secondary particle emission yield, γ, defined as the average number of the emitted particles per the incoming particle. Namely, the sputtering yield, the secondary electron emission yield and the backscattering yield are defined as the number of the sputtered particles, the secondary electrons and the backscattered particles per the incoming particle, respectively.

The phenomena of the electron emissions induced by particle impact on the solid surfaces were discovered at the beginning of this century [T 1904], [R 1905]. Since then both experimental and theoretical investigations have been done vigorously. In general, the secondary particle emission yields are found to be very sensitive to the surface conditions. In order to perform such experimental studies, one requires the ultra-high-vacuum systems, the cleaning and the characterization of the target surfaces. In the last 20 years, owing to the development of various techniques, a considerable number of reliable experimental studies on the secondary electron emission yields induced by particle impact have been made for metal targets at low energies [PPG 1969], [CCO 1969], [C 1971], [BAO 1979], [ABF 1979], [ABF 1980], [ZB 1984], [ZB 1985], [LAW 1989-a], [LAW 1989-b] and at medium-to-high energies [E 1968], [M 1975], [SH 1981], [HSB 1981], [HLS 1981], [KSS 1981], [V 1982]. The mechanisms have been understood quite well for metal targets, as will be described in Chapter 2. There are only a few investigations for alkali-halides [BPG 1971], [KKR 1975] and oxides [SW 1972], [DS 1975], [BMB 1988]. Therefore, the secondary electron emission mechanisms have not been well established for non-metallic surfaces.

Although the secondary ion emission has been extensively employed for applications such as the secondary ion mass spectrometry (SIMS), there have been only a few quantitative investigations for the secondary ion emission yields from surfaces. According to a review by Benninghoven [B 1975], the secondary ion emission yields from clean metals are usually very low (for example, $10^{-3}\sim10^{-4}$ for 3 keV Ar^+ ion impact), but those from oxygen-covered surfaces increase by 2-3 orders of magnitude (see Appendix 1). This indicates that a considerable fraction of sputtered particles is positively charged. The enhancement of the ion emission yields for oxygen-covered surfaces has been not well understood quantitatively yet.

The purpose of the present study is to reveal any differences and similarities in the interactions of ions with *metal* and *non-metallic* surfaces and to understand the related phenomena by measuring the secondary electron emission yields and the secondary positive ion emission yields under low energy ion impact on non-metallic surfaces. As will be shown later in Chapter 3, these secondary charged particle emission yields have been obtained through the measurements of the incident and emitted particle current and can be defined as

$$\gamma^- = \frac{|I_c|}{|I_i|} \qquad I_c < 0 \qquad (1\text{-}1)$$

$$\gamma^+ = \frac{|I_c|}{|I_i|} \qquad I_c > 0 \qquad (1\text{-}2)$$

where I_c is the charged particle current emitted from the target and collected at the cup and I_i the incident ion current onto the target. Here, it is assumed that negative ions and multi-charged ions emitted from targets are small and can be neglected. The validity of this assumption will be discussed in Chapter 3. Therefore, γ^- and γ^+ in the present study correspond to the secondary electron emission yields and the secondary emission yields of single charged positive ions, respectively.

Such studies are of great importance not only in basic physics but also in various applied fields. For example, the particle-induced electron emission is utilized for particle detectors and the scanning electron microscopy (SEM). The ejection of electrons, atoms and ions is one of the important problems to understand the interactions between the plasma and the wall in the fusion devices. The secondary electron emission complicates all measurements of particle currents in particle-irradiation experiments. Furthermore, in the etching processes for very large scale integrated circuits (VLSI) technology, it is a serious problem that the effect of the charge-accumulation on the insulation layers affects the accuracy and reliability of the products.

In Chapter 2, a brief discussion is given for theories and models of the secondary electron emission yields mainly for metal targets. Chapter 3 describes the present experimental apparatus and methods and also some results obtained in test experiments performed at clean Cu surfaces. The experimental results of the secondary charged particle emission yields and of mass and energy analysis of the secondary ions emitted are given in Chapter 4 and Chapter 5, respectively. Chapter 6 discusses the observed γ^- and γ^+. Finally, in Chapter 7 the observed results in the present work are summarized.

References

[ABF 1979] E. V. Alonso, R. A. Baragiola, J. Ferrón and A. Oliva-Florio, Rad. Effects 45 (1979) 119

[ABF 1980] E. V. Alonso, R. A. Baragiola, J. Ferrón, M. M. Jakas and A. Oliva-Florio, Phys. Rev. B 22 (1980) 80

[B 1975] A. Benninghoven, Surf. Sci. 53 (1975) 596

[BAO 1979] R. A. Baragiola, E. V. Alonso and A. Oliva-Florio, Phys. Rev. B 19 (1979) 121

[BMB 1988] J. E. Borovsky, D. J. Mccomas and B. L. Barraclough, Nucl. Inst. Meth. B30 (1988) 191

[BPG 1971] J. C. Baboux, M. Perdrix, R. Goutte and C. Guilland, J. Phys. D: Appl. Phys. 4 (1971) 1617

[C 1971] E. R. Cawthron, Aust. J. Phys. 24 (1971) 859

[CCO 1969] E. R. Cawthron, D. L. Cotterell and M. Oliphant, Proc. Roy. Soc. Lond. A 314 (1969) 39

[DS 1975] L. A. Dietz and J. C. Sheffield, J. Appl. Phys. 46 (1975) 4361

[E 1968] R. I. Ewing, Phys. Rev. 166 (1968) 324

[HLS 1981] D. Hasselkamp, K. G. Lang, A. Scharmann and N. Stiller, Nucl. Instr. Meth. 180 (1981) 349

[HSB 1981] G. Holmén, B. Svensson and A. Burén, Nucl. Instr. Meth. 185 (1981) 523

[KKR 1975] W. König, K. H. Krebs and S. Rogaschewski, Int. J. Mass Spectrometry and Ion Physics 16 (1975) 243

[KSS 1981] A. Koyama, T. Shikata and H. Sakairi, Jpn. J. Appl. Phys. 20 (1981) 65

[LAW 1989-a] G. Lakits, F. Aumayr and H. Winter, Europhys. Lett. 10 (1989) 679

[LAW 1989-b] G. Lakits, F. Aumayr and H. Winter, Rev. Sci. Instr. 60 (1989) 3151

[M 1975] R. G. Musket, J. Vac. Sci. Technol. 12 (1975) 444

[PPG 1969] M. Perdrix, S. Paletto, R. Goutte and C. Guillaud, Brit. J. Appl. Phys. (J. Phys. D) 2 (1969) 441

[R 1905] E. Rutherford, Phil. Mag. 10 (1905) 193

[RL 1990] G. G. Ross and L. Lebleanc, Nucl. Instr. Meth. B48 (1990) 134

[SH 1981] B. Svensson and G. Holmén, J. Appl. Phys. 52 (1981) 6928

[SW 1972] J. D. Stein and F. A. White, J. Appl. Phys. 43 (1972) 2617

[T 1904] J. J. Thomson, Proc. Cambr. Phil. Soc. 13 (1904) 49

[V 1982] E. Veje, Nucl. Instr. Meth. 194 (1982) 433

[ZB 1984] P. C. Zalm and L. J. Beckers, Philips J. Res. 39 (1984) 61

[ZB 1985] P. C. Zalm and L. J. Beckers, Surf. Sci. 152/153 (1985) 135

Chapter 2 Theoretical aspects of secondary particle emissions

In this chapter, firstly the mechanisms of the secondary electron emission yields are described and those of the secondary positive ion emission yields are briefly mentioned.

The mechanisms of ion-induced electron emission can be divided into two processes [LAH 1990]: one is the secondary electron emission induced by the kinetic energy of the incident ions and another is that induced by their potential energy [LAW 1989]. We can write the total emission yields as the sum of these two processes:

$$\gamma^- = \gamma_K^- + \gamma_P^- \qquad (2\text{-}1)$$

where γ^-_K is the *kinetic emission* yield and γ^-_P is the *potential emission* yield.

Hagstrum et al. [HL 1953], [H 1954], [H 1956] and Lander [L 1953] have studied the potential emission for metal targets. If the potential energy of the incident ion is larger than twice of the work function of the target material, the potential emission is possible through an Auger transition with one electron being captured by the projectile and the second target electron being ejected into vacuum. Kishinevsky [K 1973] has theoretically derived the following expression:

$$\gamma_P^- = \frac{0.2}{E_F}\left(0.8E_I - 2\Phi\right), \qquad (2\text{-}2)$$

where Φ and E_F are the work function and the Fermi energy of target, respectively, and E_I the ionization energy of the incident ion. On the other hand, using experimental results available for single-charged rare gas ions on various metals, Baragiola et al. [BAF 1979] have found the following empirical formula for γ^-_P:

$$\gamma_P^- = 0.032\left(0.78E_I - 2\Phi\right). \qquad (2\text{-}3)$$

The constant of 0.032 (eV^{-1}) is reasonable because E_F is several eV for many metals. These formulae tell us that the potential emission induced by the charged

ion impact on metal targets has a linear dependence on E_I and Φ. As expected, γ_K is dominant at high kinetic energies, meanwhile at very low energies γ_P is expected to become dominant.

Recently, the contribution of the potential energy to electron emission has been studied [KAS 1994] extensively in multi-charged projectile ions which have very large potential energy up to a few 100 keV. From such work the secondary electron emission yields are known to be generally larger by a factor of 2-3 than the number of the charges of the incident ions [KAS 1994].

Several theories have been developed on the *kinetic emission* of the secondary electrons from surfaces. In all theories, it is assumed that the mechanisms of the *kinetic emission* of the secondary electrons consist of the following three steps:

1) generation of electrons in the solid by kinetic energy deposition from the incoming particles,

2) transfer of these electrons towards the solid surfaces,

3) escape through the surface into vacuum.

Many processes contribute to the generation of free electrons in the solid, for example, excitation and ionization of target electrons from the conduction band and from the outer as well as inner-shells, plasmon decay and recoil ionization which is induced by energetic recoil atoms due to the elastic collisions of the incident particles. The contribution of plasmon decay is insignificant at the present collision energy range. A few theoretical studies have treated these different processes separately. It has been observed that the electron emission yields and the electronic stopping powers have nearly the same dependence on the incident ion energy. This suggests that a constant fraction of the electronic energy deposited by ions, independent of the ion impact energy, contribute to the secondary electron emissions.

These electrons, on the way to the surfaces, may collide with other electrons of target atoms and give a part of their kinetic energy to them. In consequence, it is possible that a large number of electrons are liberated through such cascade processes. In some sophisticated theories the diffusion process of electrons is

described with the mean free-paths for elastic and inelastic collisions of electrons. In the semi-empirical models, the probability of arriving at the surface for electrons which are generated at a depth X from the surface with the kinetic energy E_i is simply approximated by

$$f(X,E_i) \propto \exp\left(-\frac{X}{l(E_i)\cos\theta}\right), \qquad (2\text{-}4)$$

where θ is the angle between the electron path toward the surface and the surface normal direction and $l(E_i)$ the mean-free path of the electrons which generally depends on the electron energy and the target material. But $l(E_i)$ is often assumed to be independent of the electron energy and a constant L. In many semi-empirical treatments, the distributions of electrons generated in solids are assumed to be isotropic since the experimentally observed angular distributions of the emitted electrons into vacuum closely follow a cosine law [ST 1981].

These electrons near solid surfaces are emitted into vacuum, when they overcome the potential barrier W at the surface. W is given by sum of the workfunction Φ and the Fermi energy E_F, namely $W = E_F + \Phi$ [S 1980]. Penetration of secondary electrons through the surface barrier is treated as a refraction phenomenon. Assuming the isotropic distributions of the secondary electrons inside solid, the escape probability $P(E_i)$ for the penetration through the surface barrier can be given as

$$P(E_i) = 1 - \frac{W}{E_i} = \left(1 + \frac{W}{E_o}\right)^{-1} \quad \text{for} \quad E_i \geq W \qquad (2\text{-}5)$$

where E_i is the electron energy inside solid and $E_o = E_i - W$ is the electron energy in vacuum.

Baragiola et al. [BAF 1979], [BAO 1979] had adapted a semi-empirical theory of the secondary electron emission induced by electron impact to that for energetic ion impact and derived the following formula for the secondary electron

emission yields:

$$\gamma_K^- = \frac{PL}{2J}\left(\frac{dE}{dX}\right)_e = \Lambda_-\left(\frac{dE}{dX}\right)_e \qquad (2\text{-}6)$$

where P is the mean escape probability by overcoming the surface barrier, L the mean free path for electrons in solid, J the mean energy for producing a free electron within solid, $(dE/dX)_e = S_e$ the electronic stopping power of ions for solid, E the incident ion energy. Though P, L and J, and consequently Λ_- depend on the target materials, most of experiments suggest that Λ_- for proton impact on clean metal targets depends weakly on target materials and is close to 0.01 (nm/eV) (see Appendix 2).

Therefore the proportional coefficient Λ_- relating with the electronic stopping power and γ^- should give the important information. In Chapter 6, the proportional coefficients Λ_- for non-metallic samples are compared with those for metal samples.

The secondary positive ions are the ionized components of the sputtered atoms. There are some ideas for the ionization mechanism of the sputtered atoms: 1) the electron promotion model in which the inner-shell excitation can occur through energetic collisions and these excited atoms are ionized by autoionization mechanism, 2) the bond-breaking model in which it is assumed that charge exchange can happen at the crossings of the diabatic covalent potential curves and the diabatic ionic potential curves at a distance from the surface and 3) the dissociation model of the sputtered excited molecules and so on. However, sufficient understanding on which ionization mechanism is dominant for the secondary ions emitted from solid surfaces has not been obtained yet.

References

[BAF 1979] R. A. Baragiola, E. V. Alonso, J. Ferron and A. Oliva-Florio, Surf. Sci. 90 (1979) 240

[BAO 1979] R. A. Baragiola, E. V. Alonso and A. Oliva-Florio, Phys. Rev. B 19 (1979) 121

[H 1954] H. D. Hagstrum, Phys. Rev. 96 (1954) 325

[H 1956] H. D. Hagstrum, Phys. Rev. 104 (1956) 672

[HL 1953] H. D. Hagstrum and J. J. Lander, Rev. Sci. Instr. 24 (1953) 331

[K 1973] L. M. Kishinevsky, Rad. Eff. 19 (1973) 23

[KAS 1994] H. Kurz, F. Aumayr, D. Schneider, M. A. Briere, J. W. McDonald and HP. Winter, Phys. Rev. A 49 (1994) 4693

[L 1953] J. J. Lander, Phys. Rev. 91 (1953) 1382

[LAH 1990] G. Lakits, F. Aumayr, M. Heim and H. Winter, Phys. Rev. A, 42 (1990) 5780

[LAW 1989] G. Lakits, F. Aumayr and H. Winter, Rad. Eff. and Def. in Solids 109 (1989) 129

[S 1980] J. Schou, Phys. Rev. B, 22 (1980) 2141

[ST 1981] P. Sigmund and S. Tougaard, *Inelastic Particle-Surface Collisions* (Eds. E. Taglauer and W. Heiland, Springer-Verlag, Berlin, Heidelberg), in Chemical Physics Series 17 (1981) 2

Chapter 3 Experimental techniques

3-1 Introduction

As mentioned in Chapter 1, the secondary particle emission yield, γ, is one of the most fundamental quantities. A conventional method is measurement of the electrical current of the secondary charged particles. This method is simple and widely used. Measurements of the number distributions of the emitted electrons have also been developed recently [DS 1973], [LAW 1989-a], [LAW 1989-b]. In the present study, the former method of the current-measurement with a cup has been employed. In the negative current measurement for obtaining the secondary electron emission yield, there may be some negative ion contribution. However, this is not the case in the present work as discussed below.

The secondary electron emission yields from a clean Au surface induced by low energy proton impact measured by Baragiola et al. [BAO 1979] using a cup are found to be in good agreement with those by Lakits et al. [LAW 1989-b] who measured the number distributions of the emitted electrons using a solid state detector. It should be noted that the secondary negative ions emitted from the target, if any, could not be detected in their setup since a gold layer (about 50 nm) on the front surface of the detector is too thick for low energy secondary ions to penetrate. Therefore, it is safely assumed that the contribution of negative ions from the clean metal target is insignificant and, therefore, the observed γ^- with the current measurement is equal to the secondary electron emission yields.

Furthermore, as will be shown in Chapter 6, the observed secondary electron emission yields are approximately proportional to the electronic stopping power, indicating that the negative ion emission yields are negligibly small, compared with the secondary electron emission yields for non-metallic targets used in the present study. It should be noted that the negative ion contribution is expected to be nearly proportional to the nuclear stopping power.

In the positive current measurement, the contribution of multi-charged ions

should also be considered. According to Yu [Y 1991], the ratios of the multi-charged ion emissions to the single-charged ion emissions from Si and Ta targets were 10^{-3} and 10^{-5}, respectively. In the present study, as will be shown in Chapter 5, the multi-charged ions from the target are not observed. Consequently, one can assume that multi-charged ions emitted from target can be neglected and the observed γ^+ corresponds to the secondary positive single-charged ion emission yields. The contribution of the secondary electron emissions from the inner wall of the cup under impact of neutral and charged particles scattered from the target will be discussed in Chapter 6.

Furthermore, the mass and energy analyses of the secondary ions emitted from solid surfaces are performed using two different techniques: One is the collector method using graphite and beryllium sheets which were analyzed with Rutherford backscattering technique by 1.8 MeV helium ions and another is the mass and energy analysis with a quadrupole mass spectrometer attached with four meshes, on which the retarding voltage is applied for kinetic energy selection.

3-2 Total secondary charged particle emission yields

In the present study, an off-centered duo-plasmatron ion source has been used [TSS 1964] in order to produce low energy ($\leqq$2.5 keV) ions. This "off-centered" type sources are known to produce negative hydrogen ions with reasonable intensities [CG 1965]. After the charge and mass selection by a Wien filter, the ions were bent 90 degrees by an electrostatic quadrupole-deflector [Z 1977], which was also able to select the energy, and directed into a collision chamber after collimated to 3 mm in diameter (see Fig. 3-1 (a)).

Since the secondary particle emissions are known to depend strongly on the sample surface conditions, the following conditions should be satisfied in the experimental studies: 1) ultra-high-vacuum for contamination-free surfaces "during" measurements, 2) surface cleaning and 3) characterization of the surfaces.

The present vacuum system consists of two chambers; the preparation chamber and the main chamber, as shown in Fig. 3-1 (b). A target is put on an XYZR-manipulator and can be moved between the preparation chamber and the main chamber through a gate valve which is used to separate these two chambers. The preparation chamber is pumped down to 1×10^{-10} Torr with a turbo molecular pump with a liquid nitrogen trap. The main chamber, which is below the preparation chamber, is pumped out with an ion-pump and a titanium-sublimation-pump surrounded by a liquid nitrogen cold trap. The background pressure in the main-chamber is about 5×10^{-11} Torr without projectile beam on the target and about 1×10^{-10} Torr with projectile beam, respectively.

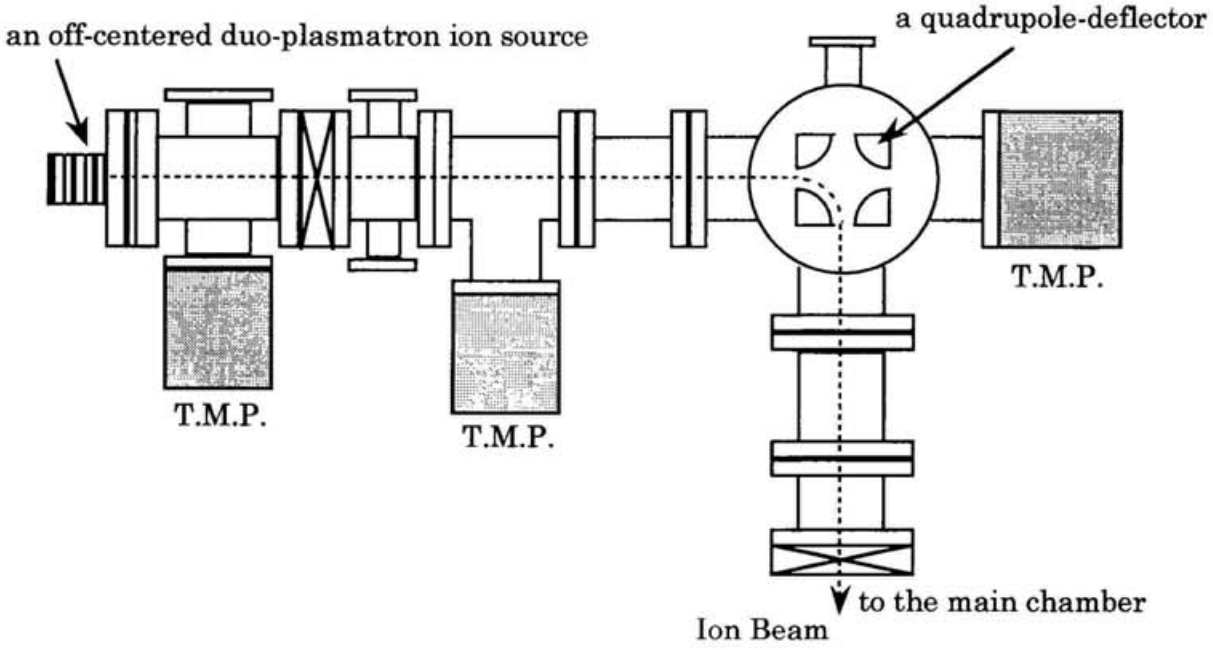

Figure 3-1 (a) A diagram of the beam line with the off-centered duo-plasmatron ion source and the quadrupole-deflector. T.M.P.: turbo molecular pump.

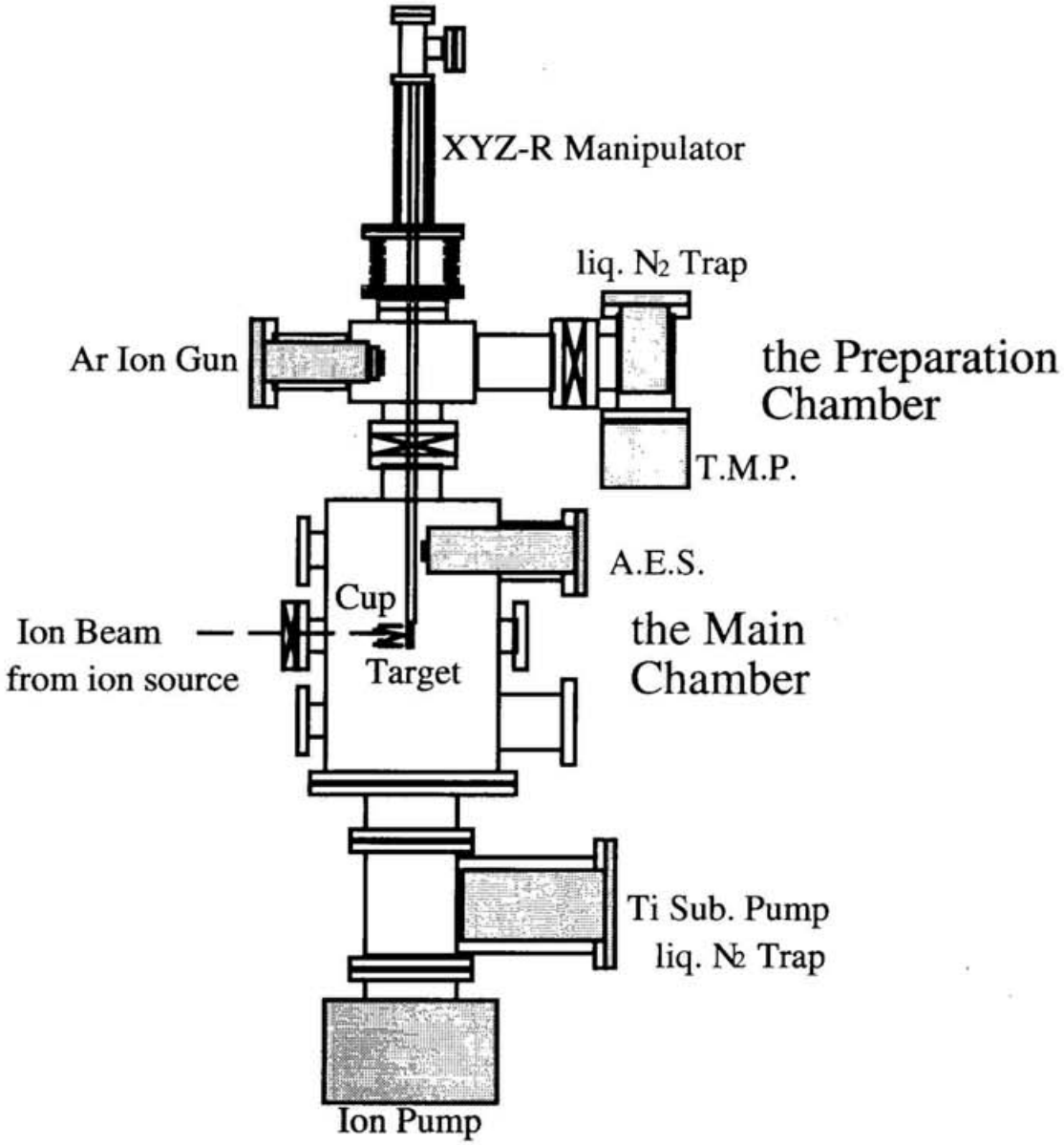

Figure 3-1 (b) A diagram of the experimental installation for the target chamber.

The target surfaces are cleaned with sputtering by Ar Ion Gun which is located at the preparation chamber (see Fig. 3-1 (b)). Also heating by a ceramic heater placed behind the target has been used, as shown in Fig. 3-2. After the targets are cleaned in the preparation chamber they are brought down into the main chamber. Then, the surface cleanness is checked by the Auger-electron-spectrometer (AES) at the main chamber. Finally the targets are brought onto the beam line at normal incident to the projectile beam.

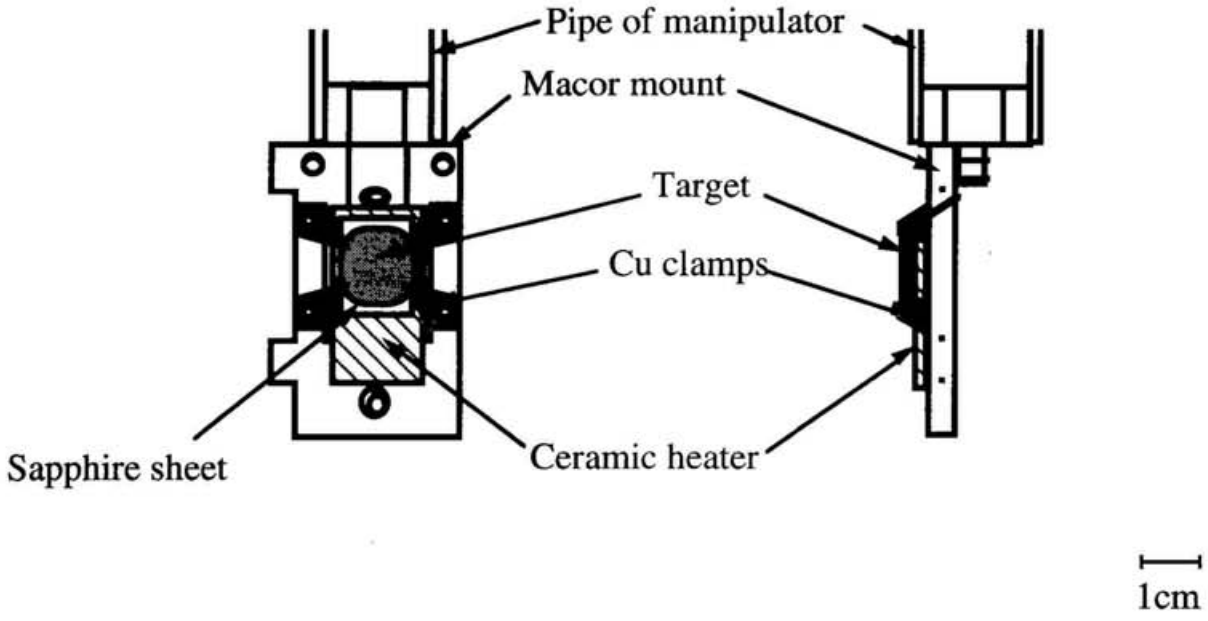

Figure 3-2 A diagram of the target and its holder. A ceramic heater can be used to heat the target up to 550 ℃. The sapphire sheet is used for electrical insulation as well as for better heat conduction from the ceramic heater.

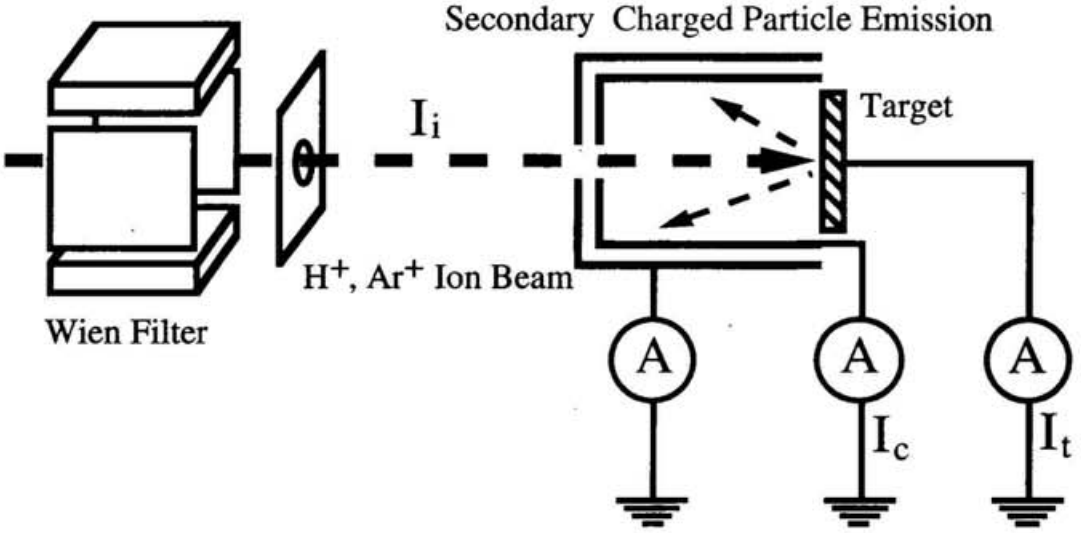

Figure 3-3 A schematic drawing of the experimental set up. The inner cup is used to measure the secondary charged particles emitted from the target and the outer cup to guard the inner cup from strayed charged particles.

Figure 3-3 shows a schematic diagram of the collection system of the secondary charged particles from a target which consists of stainless steel double cylindrical cups. The inner cup with the inner diameter of 22 mm and the length of

30 mm is used in order to collect the charged particles emitted from the target surfaces by ion impact under normal incidence conditions. The inner and outer cups have a hole of 5.5 mm and 5 mm in diameter, respectively, through which the incident ion beam collimated to about 3 mm in diameter is able to reach the target surfaces. The outer cup with the inner diameter of 32 mm and the length of 32 mm is used to protect the inner cup from strayed or scattered particles. During measurements, the current at the outer cup is also monitored to be always less than 1 % of the target current. It is possible to apply positive or negative bias potential to both the inner and outer cups. The current of both the inner cup and the target is measured with digital pico-ampere meters and then these values of the current are fed to a personal computer. In this experiment, no device such as electron bombardment for cancellation of charge-accumulation on the surfaces is employed.

High energy ion beams ($\geqq$20 keV) have been obtained using a 200 keV Cockroft-Walton type accelerator. In this high energy experiment, the vacuum of the collision chamber is $\sim 10^{-8}$ Torr.

The incident ion beam current I_i is given as the sum of the current I_t measured at the target and the current I_c measured at the inner cup, namely,

$$I_i = I_t + I_c . \qquad (3\text{-}1)$$

Then, the secondary charged particle emission yield γ is given by eqs. (1-1) and (1-2).

In the present experiment performed at the ultra-high-vacuum chamber, no significant difference is noticed for γ^- and γ^+ for $SrCeO_3$ (5 % Yb) and $YBa_2Cu_3O_7$ before and after surface cleaning. This is quite different from metal targets and one of the interesting features of these targets. Consequently, for these targets, the data obtained in the high-vacuum conditions as well as those in ultra-high-vacuum conditions can be used in comparison with the electronic stopping power (see Chapter 6).

3-3 Mass analysis by a collector method

In order to identify ions emitted from the target surfaces under ion impact, a simple collector method is used as shown in Fig. 3-4. Ion beam from 200 kV Cockroft-Walton type accelerator is introduced to the target surfaces under normal incidence conditions. Graphite and beryllium sheets are put in front of the target at ~45 degrees with respect to the incident ion direction. In order to collect effectively the secondary positive ions, the negative potential (-180V) is applied to both the collectors and also the positive potential (+90V) to the target. The incident ion current to the target and the charged particles on the collectors are also measured. In this experiment, the pressure of the collision chamber is about 10^{-7} Torr.

The ions (including neutrals) on the collector surfaces have been analyzed with Rutherford backscattering (RBS) technique using 1.8 MeV helium ions.

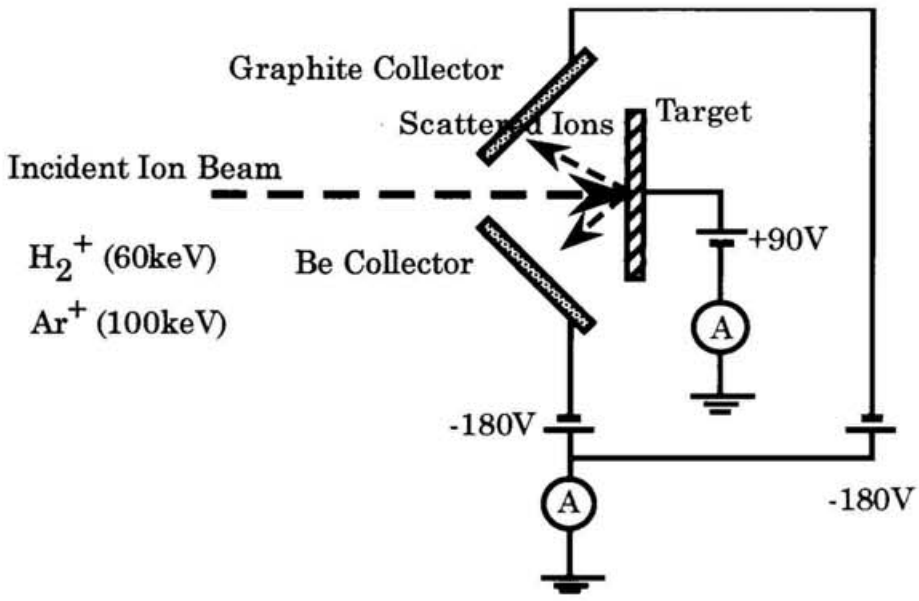

Figure 3-4 A schematic drawing of the experimental setup for collector method.

3-4 Mass and energy analysis by a quadrupole-mass-spectrometer combined with retardation technique

Figure 3-5 shows the present experimental setup where a quadrupole-mass-spectrometer (QMS) was used as an ion analyzer. This QMS is put in front of the target at normal conditions, meanwhile the incident ions strike the target surfaces at 45 degrees. The four meshes between the head of QMS and the target surface are put in order to apply the retarding potential. Thus the kinetic energy of the secondary ions can be estimated. This experiment has been carried out in the preparation chamber where larger current of the incident ion beam (without mass/charge analysis) was obtained from the ion gun used for sputter-cleaning.

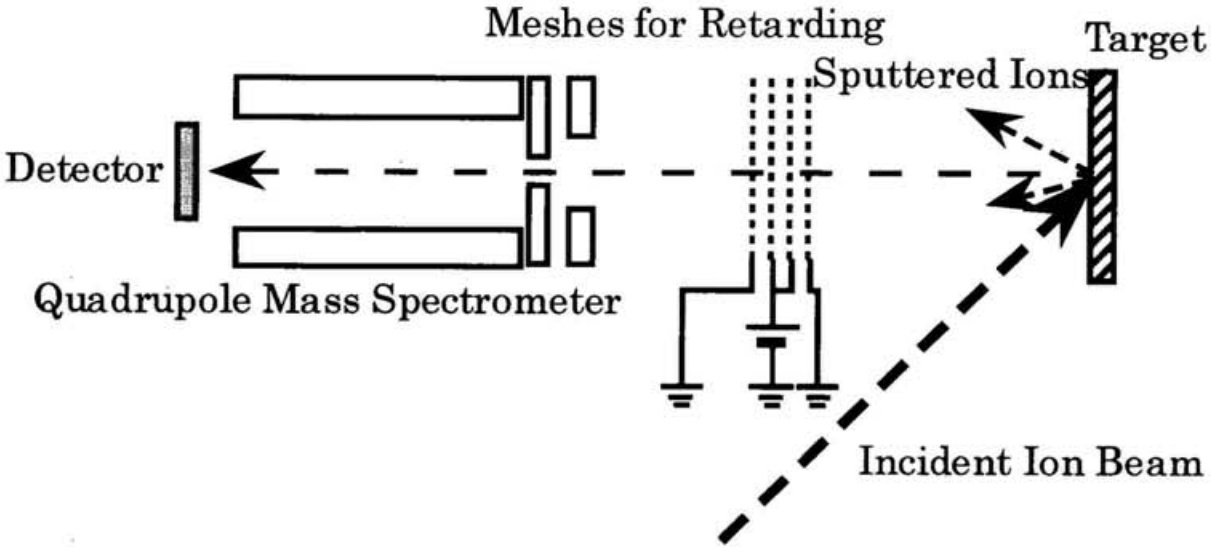

Figure 3-5 A schematic drawing of the experimental setup for mass and energy analysis using the quadrupole-mass-spectrometer.

3-5 Test of the present system using clean Cu surfaces

In order to test the present apparatus, γ^- induced by H^+ impact on clean Cu surfaces has been measured as a function of the incident H^+ energy. The positive bias potential (+9 V) is applied to the inner cup. Firstly, Cu surface was cleaned by sputtering using 3 keV Ar ions. Figures 3-6 (a) and (b) show typical Auger electron spectra from a Cu surface before sputtering and after 15 minute Ar^+ ion sputtering with the current density of 25 $\mu A/cm^2$. From these results, it is clear that the main impurities on the surfaces are O and C and Ar ion sputtering effectively removes almost all of these.

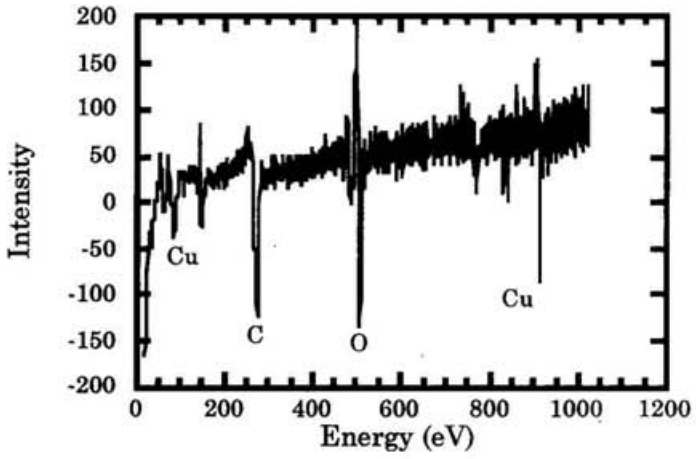

Figure 3-6 (a) A typicalAuger electron spectrum from a Cu surface before sputtering. The surface densities of O, C and Cu have been estimated to be 29.4, 41.2 and 29.3 %, respectively.

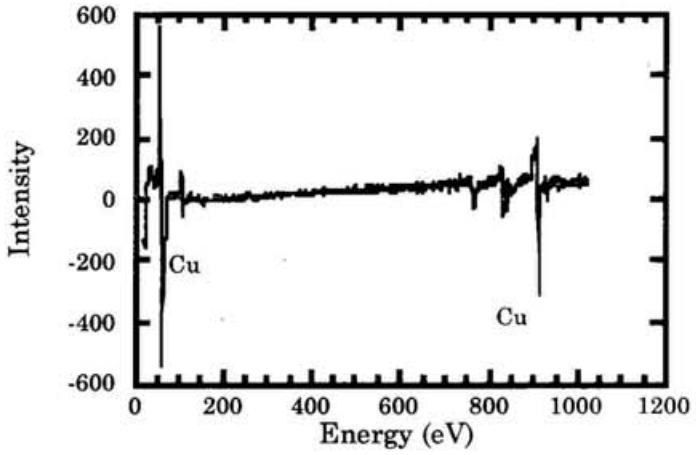

Figure 3-6 (b) A typicalAuger electron spectrum from a Cu surface after sputtering. The surface densities of O, C and Cu have been estimated to be 1.9, 4.5 and 93.6 %, respectively.

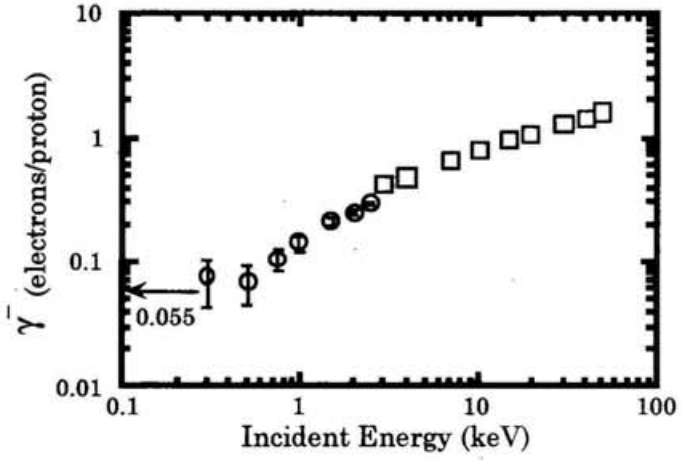

Figure 3-7 Incident energy dependence of γ^- from a clean Cu surface by H^+ impact; ○ (present work), □ (Baragiola et al.), ← shows the secondary electron emission yields due to the potential emission estimated with a formula proposed by Baragiola et al.

Figure 3-7 shows the present results of γ^- for Cu as a function of the impact energy (open circles). In this figure the experimental results at higher energies measured by Baragiola et al. [BAO 1979] are also shown with the open squares. As the ion impact energy decreases, the γ^- yield decreases and finally reaches a

constant value. As mentioned in Chapter 2, γ^- from solid surfaces under ion impact is known to be contributed from two parts: the potential emission and the kinetic emission. The constant γ^- observed in the present work at the incident ion energy below 500 eV is understood to be due to the potential emission. Using the empirical formula (2-3) introduced by Baragiola et al. [BAF 1979], the γ^-_p is estimated to be 0.055 for Cu, shown with an arrow, which is in reasonable agreement with the present results.

To get more information, the mass and energy of the secondary ions have been analyzed with a quadrupole-mass-spectrometer with four-mesh retardation electrodes. Figures 3-8 (a)-(d) show the secondary ion spectra from clean Cu surfaces under 0.8 keV Ar^+ ion impact. The peak at mass 40 corresponds to Ar^+ ions which are understood to originate from the Ar atoms accumulated on the Cu target and sputtered with the subsequent Ar^+ ions. Furthermore it is noticed that this Ar ion intensity decreases as the retarding potential increases and becomes almost zero at 7 V, suggesting that the kinetic energy of the sputtered Ar^+ ions is quite small. This agrees with the expectation that most of the sputtered particles have only a few eV of the kinetic energy [H 1991].

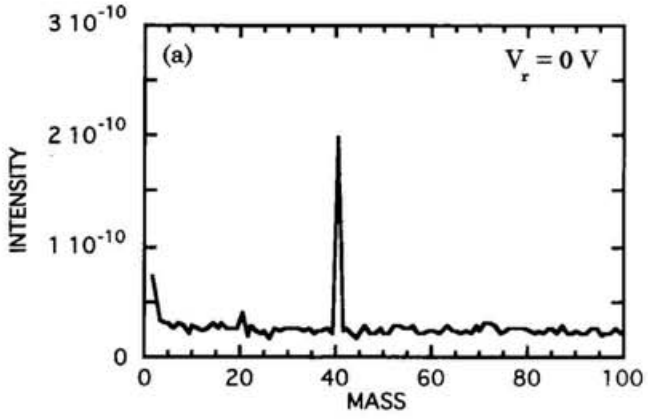

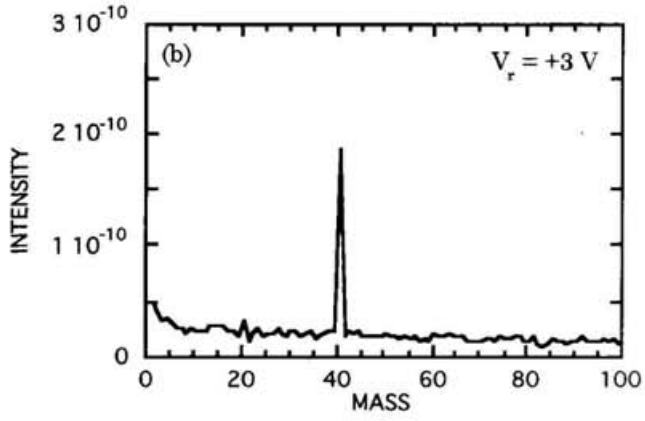

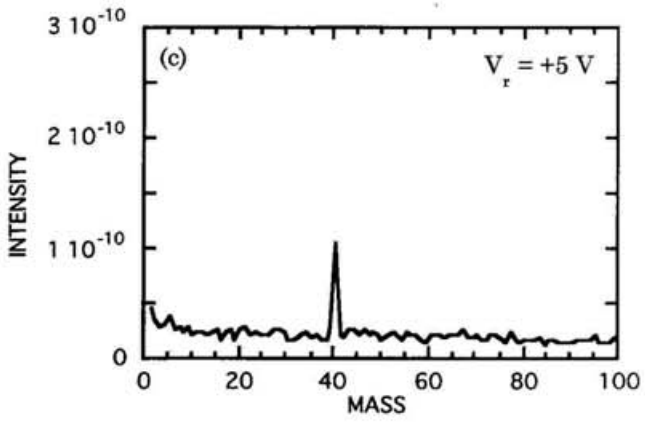

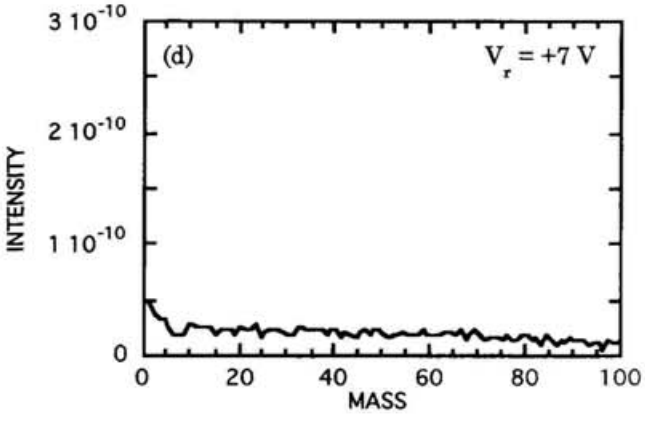

Figure 3-8 Ion mass spectra from clean Cu surfaces impacted by 0.8 keV Ar^+ ions at different retarding potential V_r applied on the retarding meshes (see Fig. 3-5). (a), (b), (c) and (d) correspond to the retarding voltage of 0, +3 , +5 and +7 V, respectively.

3-6 Properties of non-metallic targets

Three non-metallic samples, namely TiO_2, $YBa_2Cu_3O_7$ and $SrCeO_3$ (5% Yb), have been used as target. Some properties of these targets are described below.

(a) TiO_2

TiO_2 has a rutile structure which is the simplest among all the titanium oxides. The energy band gap is 3.05 eV and the electrical resistivity is over 10^{13} Ωcm at room temperatures.

(b) $YBa_2Cu_3O_7$

$YBa_2Cu_3O_7$ is one of the perovskite type oxides. This material is well known as high critical temperature superconductors. The electrical resistivity is $\sim 10^{-4}$ Ωcm at 280 K.

(c) $SrCeO_3$ (5 % Yb)

$SrCeO_3$ (5 % Yb) is also one of the perovskite type oxides. The present sample contains 5% Yb. Yb-doped $SrCeO_3$ is known to exhibit good protonic conduction in hydrogen-containing atmospheres at high temperatures (> 600 ℃) [YI 1992-a], [YI 1992-b], [HMY 1992] but, at room temperatures, has high resistivity which is very close to that of the insulator.

Table 3-1 gives the density and the surface binding energy of these targets. These parameters are used to calculate the sputtering yields for comparison with the experimental ion emission yields.

Table 3-1 The density, the surface binding energy and the resistivity of non-metallic targets used in the present study.

	density (g/cm^3)	density ($10^{22}/cm^3$)	surface binding energy (eV)	resistivity (Ω cm) at room temperatures
TiO_2	4.26	N_{Ti} 3.20	6.6	$\sim 10^{13}$
$YBa_2Cu_3O_7$	6.38	N_Y 0.577	3.0	$\sim 10^{-4}$
$SrCeO_3$ (5 % Yb)	5.82	N_{Sr} 1.27	6.1	------

N_{Ti}, N_Y and N_{Sr} show the number density of Ti, Y and Sr, respectively.

References

[BAF 1979] R. A. Baragiola, E. V. Alonso, J. Ferron and A. Oliva-Florio, Sur. Sci. 90 (1979) 240-255

[BAO 1979] R. A. Baragiola, E. V. Alonso and A. Oliva-Florio, Phys. Rev. B 19 (1979) 121

[CG 1965] L. E. Collins and R. H. Gobbett, Nucl. Instr. Meth. 35 (1965) 277

[DS 1973] L. A. Dietz and J. C. Sheffield, Rev. Sci. Instr. 44 (1973) 183

[H 1991] W. O. Hofer, *Sputtering by Particle Bombardment* III (Eds. R. Behrisch and K. Wittmaack, Springer-Verlag, Berlin, Heidelberg), Topics in Applied Physics 64 (1991) 15

[HMY 1992] T. Hibino, K. Mizutani, T. Yajima and H. Iwahara, Solid State Ionics 57 (1992) 303

[LAW 1989-a] G. Lakits, F. Aumayr and H. Winter, Europhys. Lett. 10 (1989) 679

[LAW 1989-b] G. Lakits, F. Aumayr and H. Winter, Rev. Sci. Instr. 60 (1989) 3151

[TSS 1964] H. Tawara, S. Suganomata and S. Suematsu, Nucl. Instr. Meth. 31 (1964) 353

[Y 1991] M. L. Yu, *Sputtering by Particle Bombardment* III (Eds. R. Behrisch and K. Wittmaack, Springer-Verlag, Berlin, Heidelberg), Topics in Applied Physics 64 (1991) 91

[YI 1992-a] T. Yajima and H. Iwahara, Solid State Ionics 50 (1992) 281

[YI 1992-b] T. Yajima and H. Iwahara, Solid State Ionics 53/56 (1992) 983

[Z 1977] H. D. Zeman, Rev. Sci. Instr. 48 (1977) 1079

Chapter 4 Experimental results of the secondary charged particle emission yields

The secondary electron and positive ion emission yields were measured using the method described in Chapter 3. This chapter describes the observed results for Be, BeO, TiO_2, $YBa_2Cu_3O_7$ and $SrCeO_3$ (5 % Yb).

4-1 Be / BeO

Figure 4-1 shows the inner cup bias potential dependence of γ induced by 2.5 keV proton impact on unclean BeO and it is clearly seen that γ^- is constant at the bias potential over +50 V. Hence, the positive bias potential (+50 V) was applied to the inner cup in the present measurements while γ^- is being measured. To see the surface effects, the dependence of γ^- from Be on oxidation under 2.5 keV H^+ impact have been measured. The results are shown in Figs. 4-2 (a) and (b) as a function of the ratio of oxygen-to-beryllium (O/Be) and carbon-to-beryllium (C/Be) of the target surfaces which is determined from the Auger electron spectra. In Figs. 4-2 (a) and (b), the circles and squares indicate the data from two different Be targets. A typical Auger electron spectrum before sputtering is shown in Fig. 4-3 (a) and also Figs. 4-3 (b) and (c) show typical Auger electron spectra which have been obtained after 140 and 730 minute sputtering, respectively, with 3 keV Ar^+ ions of 25 $\mu A/cm^2$. Figure 4-2 (a) shows that γ^- is roughly constant to be 2 when O/Be ratio is larger than 0.3 and, as the O/Be ratio decreases, γ^- also decreases and becomes nearly constant at the O/Be ratio below 0.02. This value at the lowest O/Be ratio is in agreement with 0.4 estimated by Thomas empirical formula [T 1995]. Furthermore, from Figs. 4-2 (a) and (b), it is noticed that γ^- depends on the O/Be ratio but practically independent of the C/Be ratio. This shows that γ^- is influenced more strongly by oxygen than by carbon.

The ratio of γ^- at large O/Be to that at clean Be is 4~5 which is roughly in

agreement with those previously measured for metal oxide surfaces [BAF 1979].

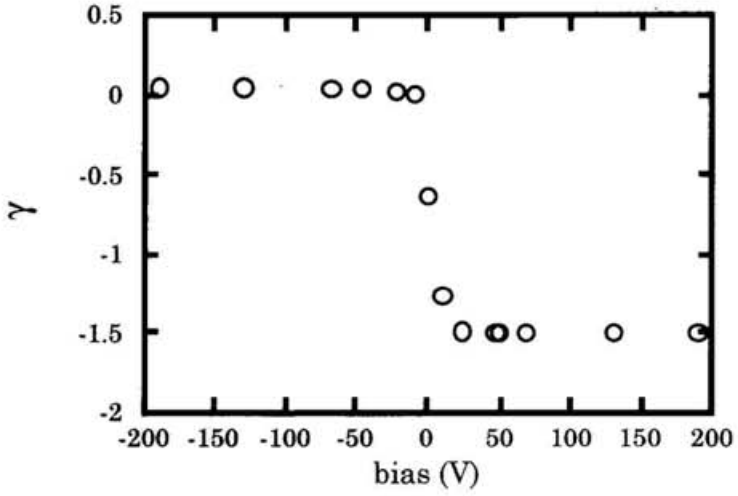

Figure 4-1 Inner cup bias potential dependence of γ induced by 2.5 keV proton impact on unclean BeO.

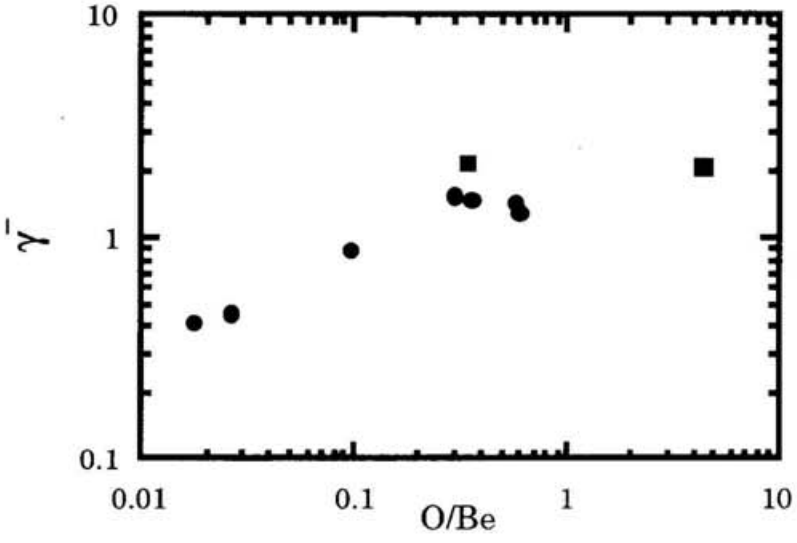

Figure 4-2 (a) γ^- from Be surfaces as a function of O/Be ratio at 2.5 keV H^+ impact. ● and ■ are taken from two different samples.

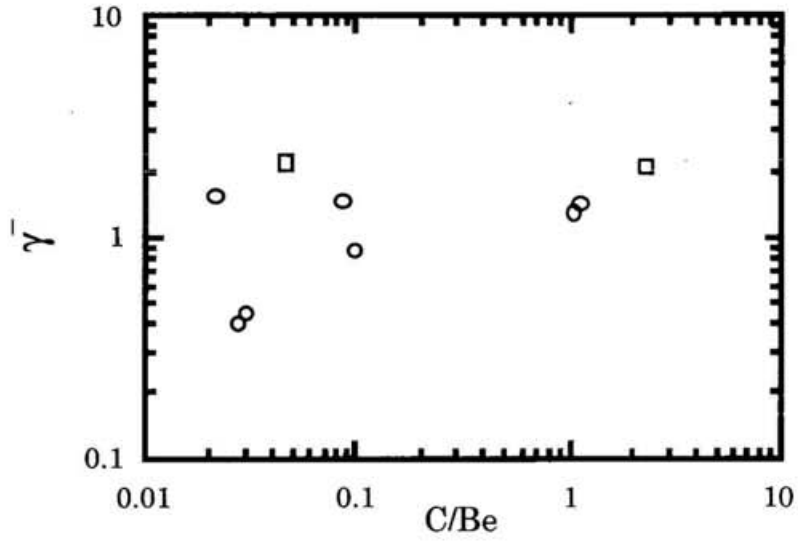

Figure 4-2 (b) γ^- from Be surfaces as a function of C/Be ratio at 2.5 keV H^+ impact. ○ and □ are taken from two different samples.

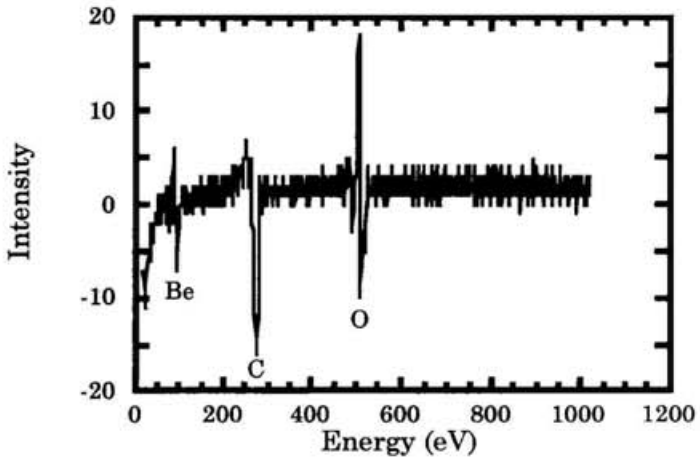

Figure 4-3 (a) A typical Auger electron spectrum from Be before sputtering by Ar ions. O/Be and C/Be ratios have been estimated to be 0.57 and 1.1, respectively.

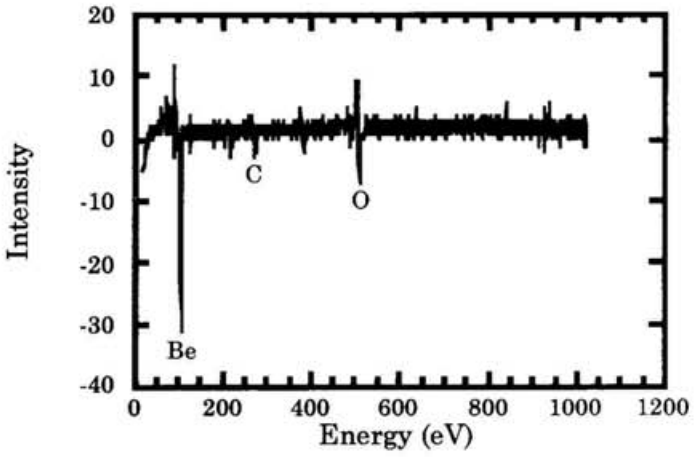

Figure 4-3 (b) A typical Auger electron spectrum from Be after 140 min. sputtering by Ar ions. O/Be and C/Be ratios have been estimated to be 0.1 and 0.096, respectively.

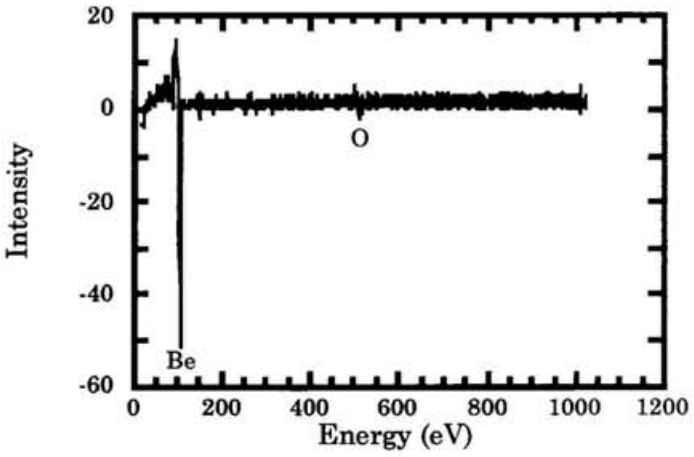

Figure 4-3 (c) A typical Auger electron spectrum from Be after 730 min. sputtering by Ar ions. O/Be and C/Be ratios have been estimated to be 0.02 and 0.03, respectively.

4-2 TiO_2

Figure 4-4 shows the inner cup bias potential dependence of γ induced by 2.5 keV proton impact on unclean TiO_2 and it is found that γ^- and γ^+ are constant at the bias potential over +50 V and below -50 V, respectively. In the present measurement, -50 V and +50 V bias potentials were applied to the inner cup for measurements of γ^- and γ^+, respectively. Figures 4-5 (a) and (b) show the observed γ^- and γ^+, respectively, under 2.5 keV H^+ ion impact on clean and unclean TiO_2 as a function of the incident ion current. From these results, it is noticed that γ^- and γ^+ are independent of the incident ion current, similar to those for metal targets. The observed γ^- is 0.33 for clean TiO_2 and 0.93 for unclean TiO_2 surfaces. This difference is similar to that observed in metal targets. On the other hand, the measured γ^+ for clean TiO_2 is nearly the same as that for unclean TiO_2 and far larger than that for metal targets as well as the sum of the sputtered and the backscattered ion yields calculated by TRIM code (see discussion in Chapter 6). Similarly, γ^- and γ^+ induced by 2.5 keV Ar^+ ion impact on clean TiO_2 were measured. It is found that γ^- and γ^+ are also independent of the incident current and 0.30 and 0.092, respectively.

Figures 4-6 (a) and (b) show typical Auger electron spectra from a TiO_2 surface before sputtering and after 10 minute sputtering by Ar^+ ion at 25 $\mu A/cm^2$. From these results, it is clear that the main impurity on the surfaces is C, though relatively weak, which is removed almost to zero by Ar^+ ion sputtering.

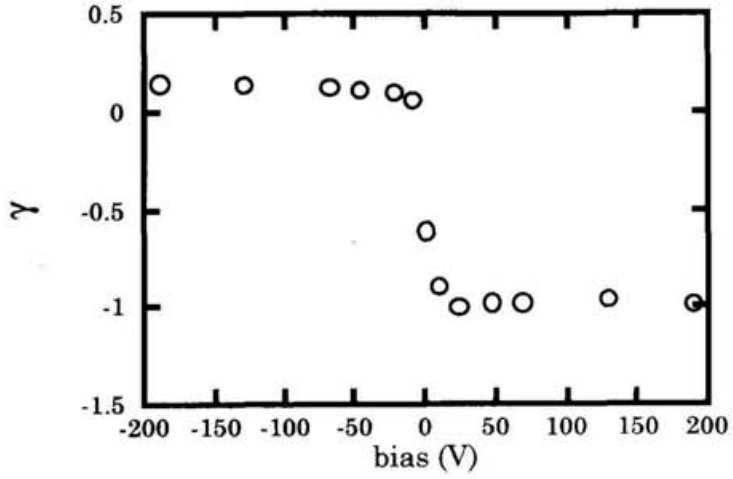

Figure 4-4 Inner cup bias potential dependence of γ induced by 2.5 keV proton impact on unclean TiO_2.

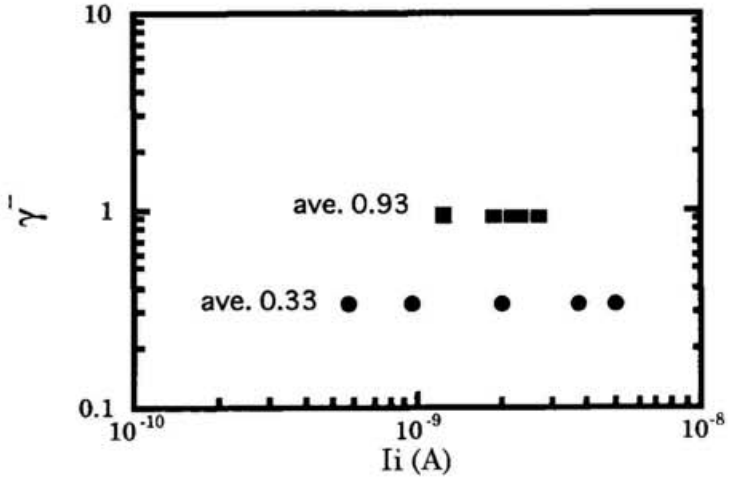

Figure 4-5 (a) Ion flux dependence of γ^- induced by 2.5 keV H^+ impact on clean (●) and unclean (■) TiO_2 surfaces. The positive potential (+50 V) is applied to the inner cup.

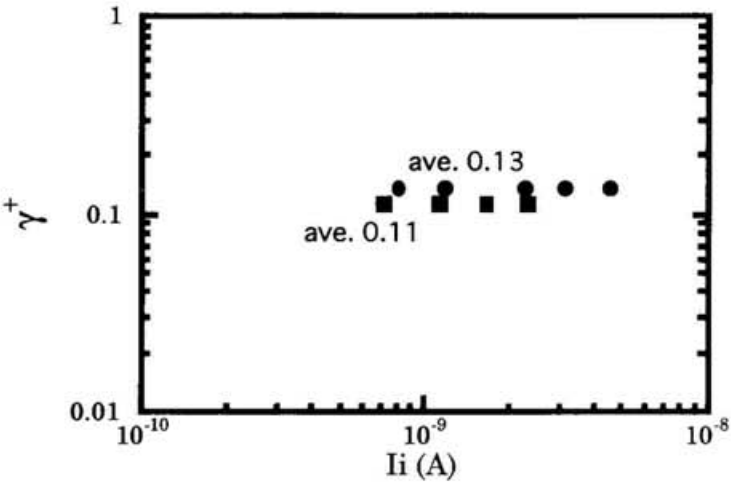

Figure 4-5 (b) Ion flux dependence of γ^+ induced by 2.5 keV H^+ impact on clean (●) and unclean (■) TiO_2 surfaces. The negative potential (-50 V) is applied to the inner cup.

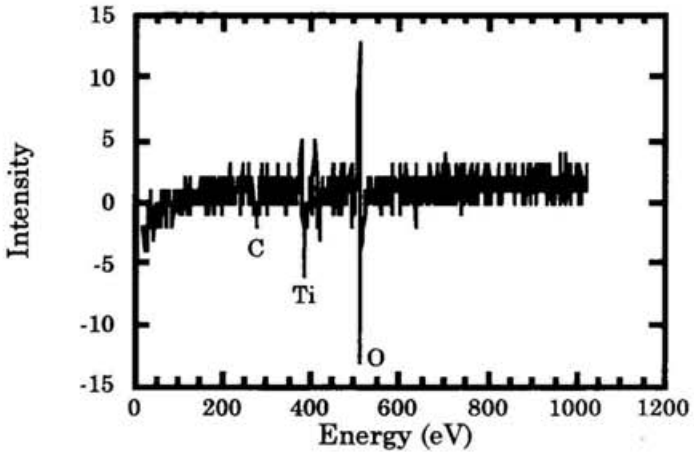

Figure 4-6 (a) A typical Auger electron spectrum from TiO_2 before sputtering by Ar^+ ions. The surface densities of C, Ti and O have been estimated to be 21.3, 22.9 and 55.8 %, respectively.

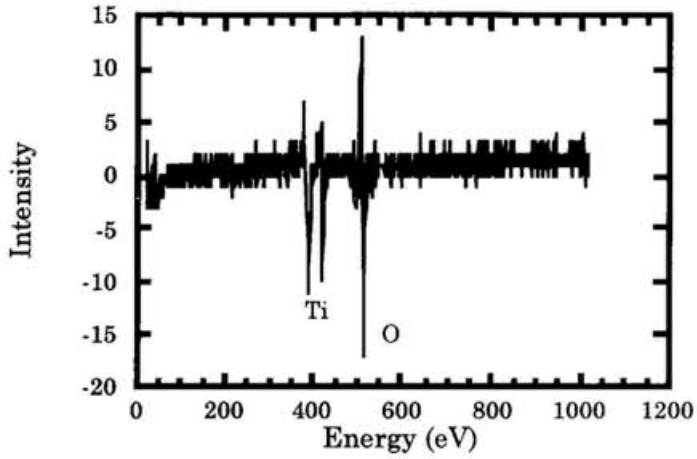

Figure 4-6 (b) A typical Auger electron spectrum from TiO_2 after sputtering by Ar^+ ions. The surface densities of C, Ti and O have been estimated to be 5.2, 39.7 and 55.1 %, respectively.

4-3 $YBa_2Cu_3O_7$

Figure 4-7 shows the inner cup bias potential dependence of γ induced by 2.5 keV proton impact on unclean $YBa_2Cu_3O_7$ and it is found that γ^- and γ^+ are constant at the bias potential over +50 V and below -50 V, respectively. In the present measurement, -50 V or +50 V bias potential was applied to the inner cup for measurements of γ^- or γ^+, respectively. Figures 4-8 (a) and (b) show the observed γ^- and γ^+ induced by 2.5 keV H^+ impact on clean and unclean $YBa_2Cu_3O_7$ as a function of the incident ion beam current. Figures 4-9 (a) and (b) show typical Auger electron spectra from $YBa_2Cu_3O_7$ surface before sputtering and after 20 minute sputtering by Ar^+ ion at 25 $\mu A/cm^2$. From these results, it is clear that the main impurity on the surfaces is also C which is removed almost to zero by Ar^+ ion sputtering.

Both γ^- and γ^+ do not depend upon the incident ion current, similar to those

for metal targets and TiO_2 target. However, the observed γ^- is much larger than that for metals and does not depend upon the surface conditions. The observed γ^+ is also larger than that for clean metal targets and the sum of the sputtering yield and the backscattering yield calculated by TRIM code (see discussion in Chapter 6). It is also found that γ^+ is also nearly the same both for clean and unclean $YBa_2Cu_3O_7$.

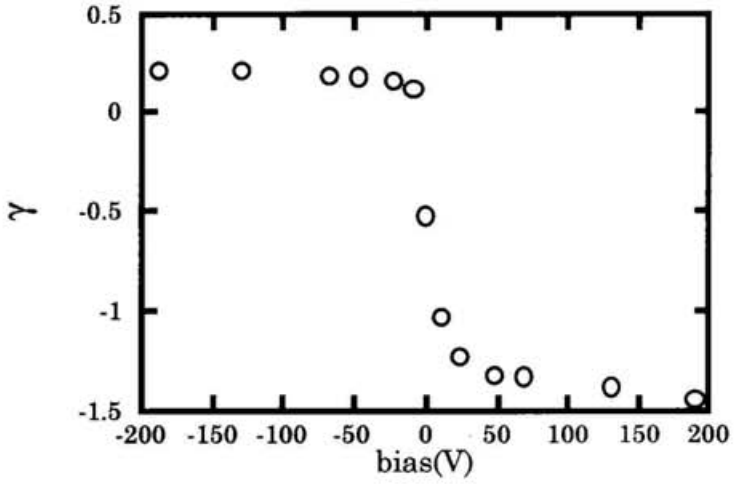

Figure 4-7 Inner cup bias potential dependence of γ induced by 2.5 keV proton impact on unclean $YBa_2Cu_3O_7$.

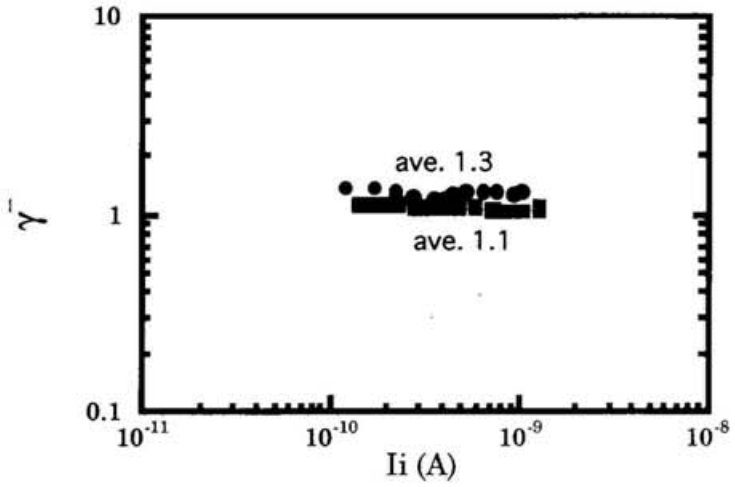

Figure 4-8 (a) Ion flux dependence of γ^- induced by 2.5 keV H^+ impact on clean (●) and unclean (■) $YBa_2Cu_3O_7$. The positive potential (+50 V) is applied to the inner cup.

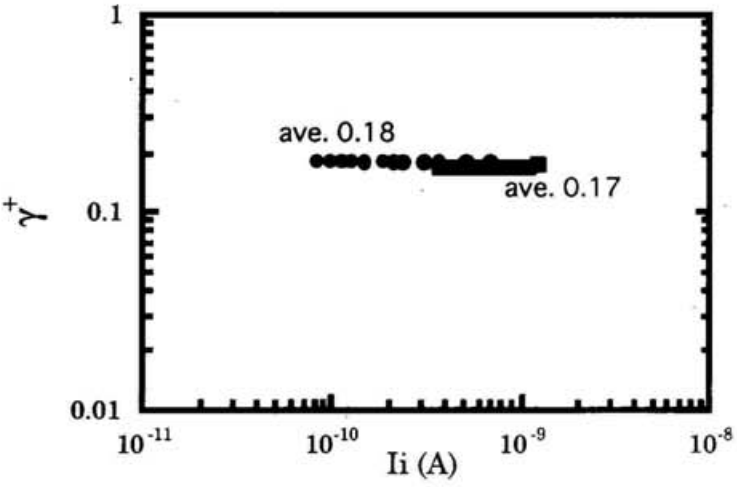

Figure 4-8 (b) Ion flux dependence of γ^+ induced by 2.5 keV H^+ impact on clean (●) and unclean (■) $YBa_2Cu_3O_7$. The negative potential (-50 V) is applied to the inner cup.

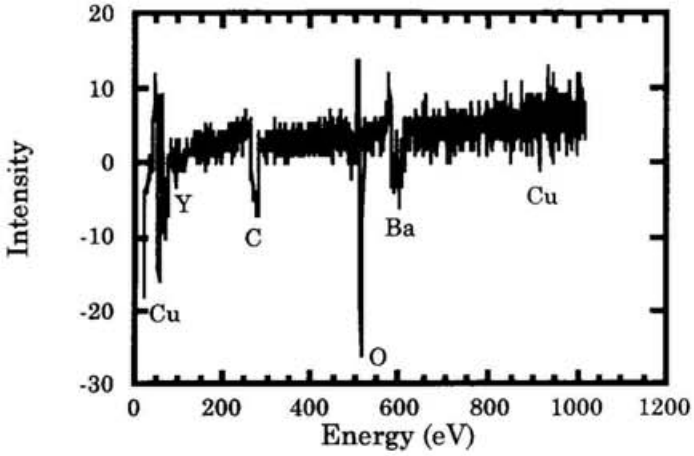

Figure 4-9 (a) A typical Auger electron spectrum from $YBa_2Cu_3O_7$ surfaces before sputtering by Ar^+ ions.

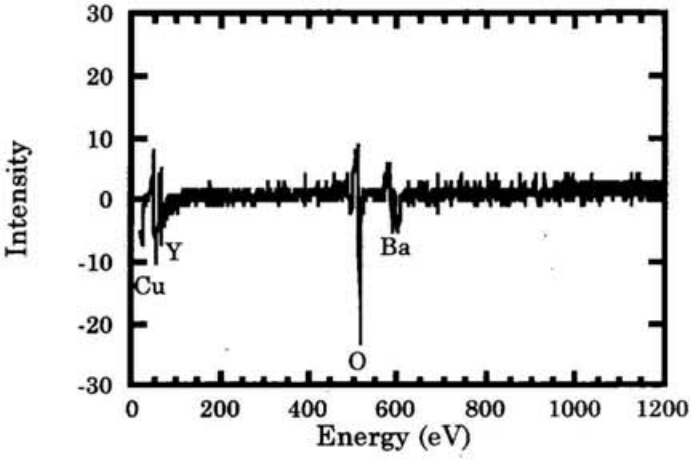

Figure 4-9 (b) A typical Auger electron spectrum from $YBa_2Cu_3O_7$ surfaces after sputtering by Ar^+ ions.

4-4 $SrCeO_3$(5 % Yb)

Figures 4-10 (a)-(f) show the observed γ^- and γ^+ under 2.5 keV H^+, H_2^+ and Ar^+ impact on unclean $SrCeO_3$ (5% Yb) surfaces as a function of the incident ion current. In these figures, the "positive" part corresponds to the secondary positive ion emission yields γ^+, meanwhile the "negative" part the secondary electron emission yields γ^-. From these results, it is noticed that γ^- measured with the positive potential (+50 V) applied to the inner cup shows a behavior which has not been known so far for any material. Interestingly, it is observed that γ^- decreases toward zero as the incident ion current increases and changes from the negative (electrons) to the positive (ions) above a critical ion current which has been found to depend upon the incident ion energy and the target temperature. These features (Fig. 4-10 (a), (c) and (e)) suggest that, for this specific material, the electron emission is dominant at low incident ion current, meanwhile it is overcome by the secondary positive ion emission at high ion current. It is also observed that γ^+ measured with the negative potential (-50 V) to the inner cup is independent of the incident ion current (see Figs. 4-10 (b) and (d)). It is noted that the observed γ^+ is not influenced by the positive potential on the inner cup (see Figs. 4-10 (a) and (b)), suggesting that the observed positive ions should have high energy. Similar results were also observed for clean $SrCeO_3$ (5% Yb).

Furthermore, γ^- induced by 2.5 keV H^- ions has been measured and shown in Fig. 4-11. In this measurement, no bias potential has been applied to the inner cup. It is noticed that there is no flux dependence in H^- impact and γ^- is about 1. This result clearly suggests that the electron, loosely bound to H atom before collisions with the surface and liberated after collision, may contribute to γ^-, possibly via reflection from the surface and practically no charge-accumulation occurs at the surfaces. This is why γ^- under H^- ion impact does not depend on the incident ion flux.

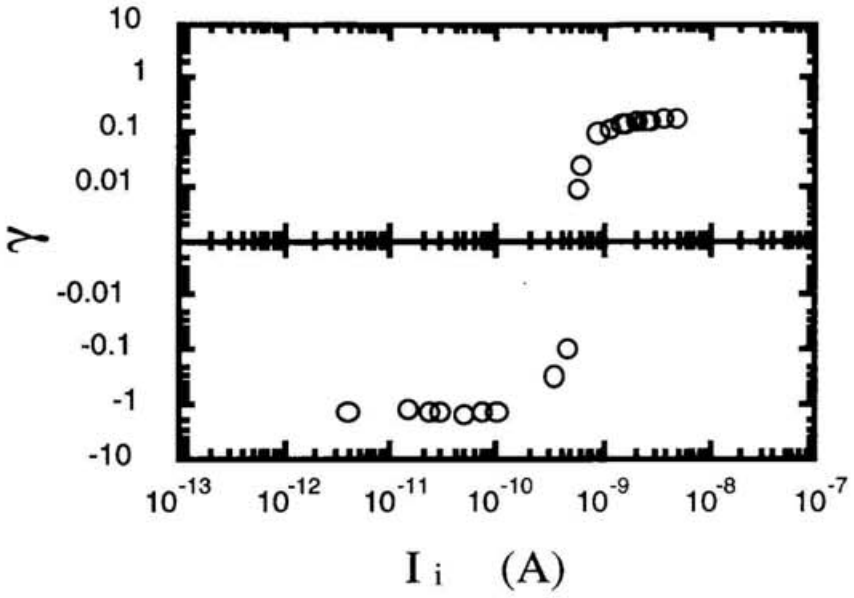

Figure 4-10 (a) Ion-flux dependence of γ induced by 2.5 keV H^+ impact on $SrCeO_3$ (5 % Yb). The positive potential (+50 V) is applied to the inner cup.

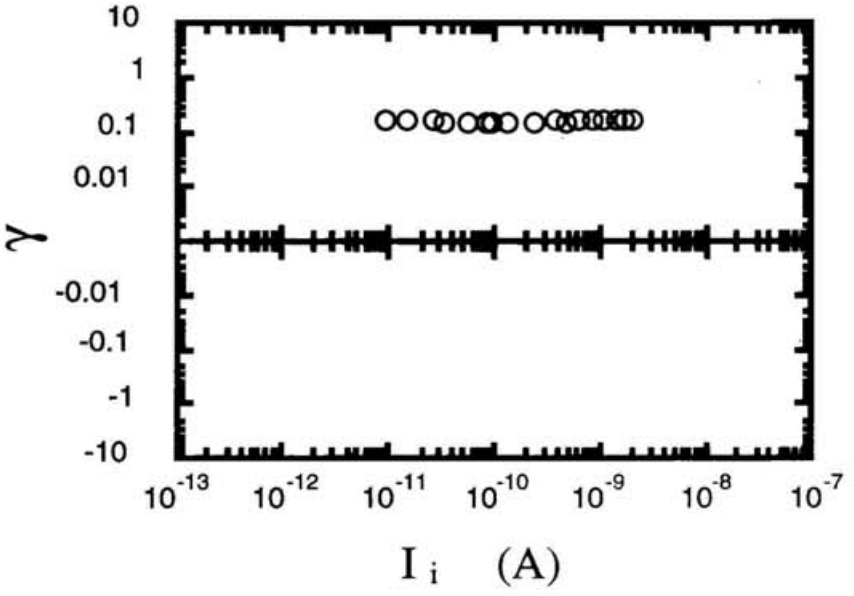

Figure 4-10 (b) Ion-flux dependence of γ^- induced by 2.5 keV H^+ impact on $SrCeO_3$ (5 % Yb). The negative potential (-50 V) is applied to the inner cup.

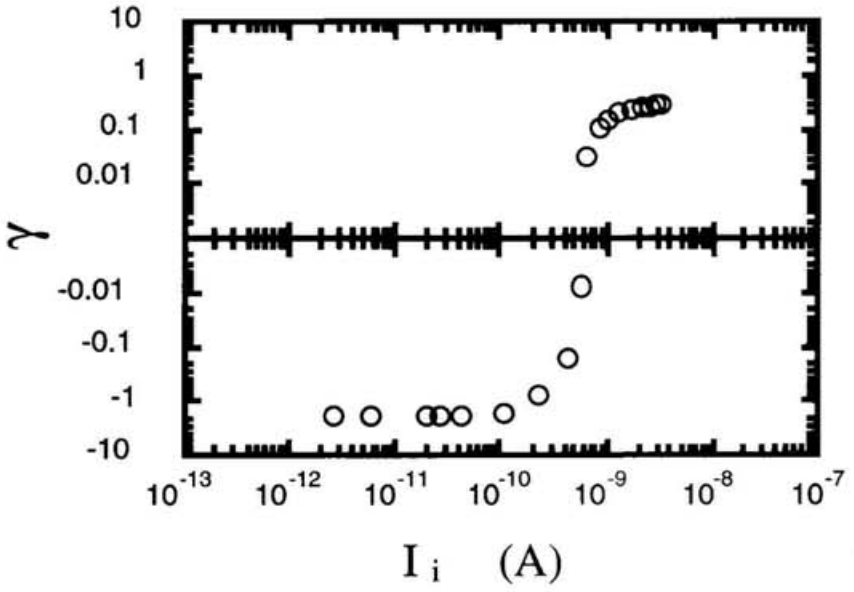

Figure 4-10 (c) Ion-flux dependence of γ induced by 2.5 keV H_2^+ impact on $SrCeO_3$ (5 % Yb). The positive potential (+50 V) is applied to the inner cup.

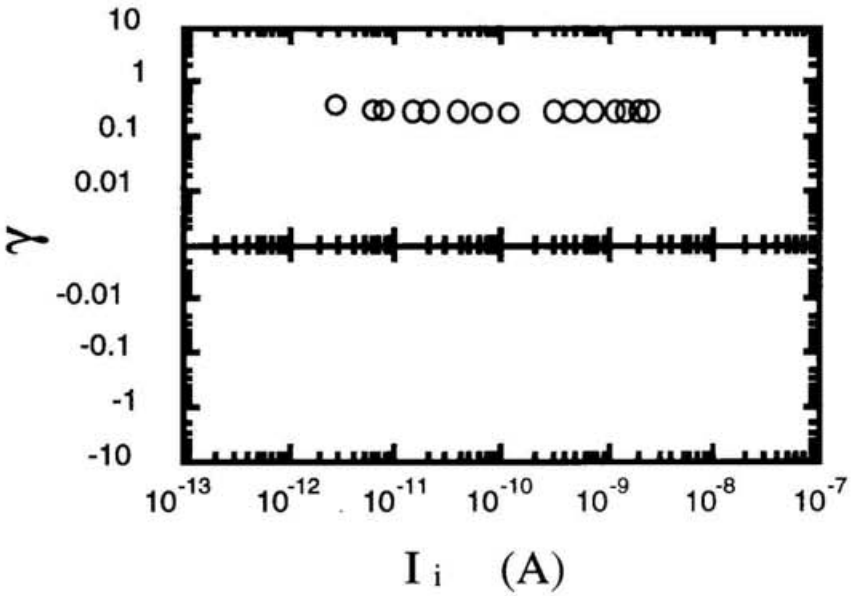

Figure 4-10 (d) Ion-flux dependence of γ^+ induced by 2.5 keV H_2^+ impact on $SrCeO_3$ (5 % Yb). The negative potential (-50 V) is applied to the inner cup.

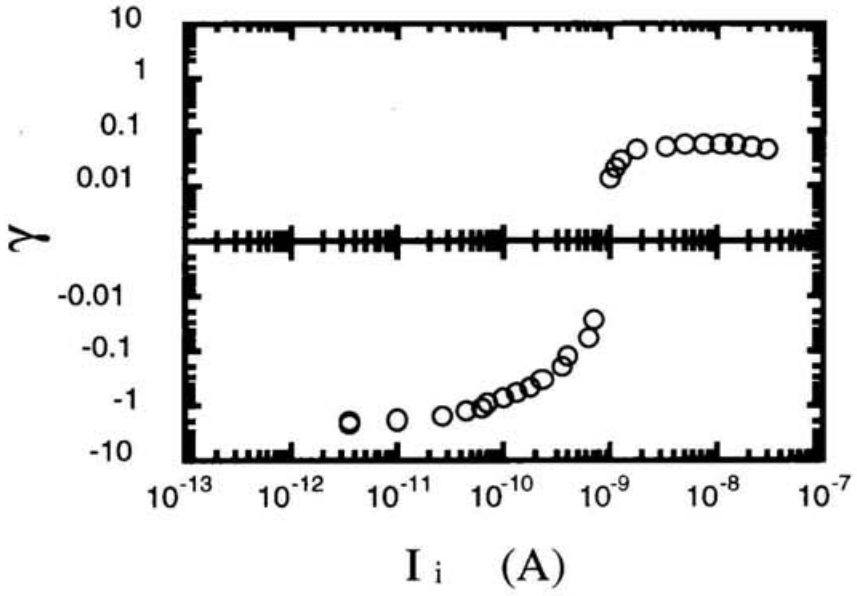

Figure 4-10 (e) Ion-flux dependence of γ induced by 2.5 keV Ar^+ impact on $SrCeO_3$ (5 % Yb). The positive potential (+50 V) is applied to the inner cup.

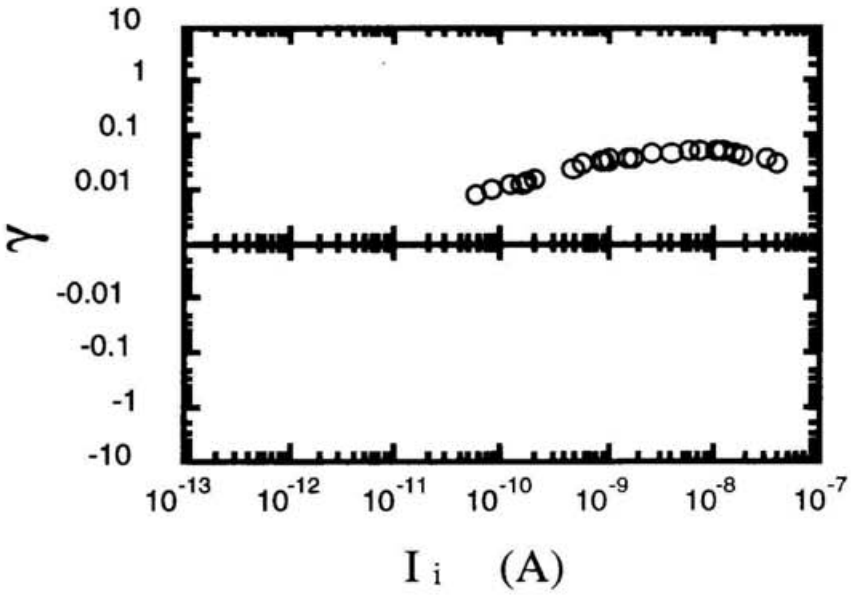

Figure 4-10 (f) Ion-flux dependence of γ^+ induced by 2.5 keV Ar^+ impact on $SrCeO_3$ (5 % Yb). The negative potential (-50 V) is applied to the inner cup.

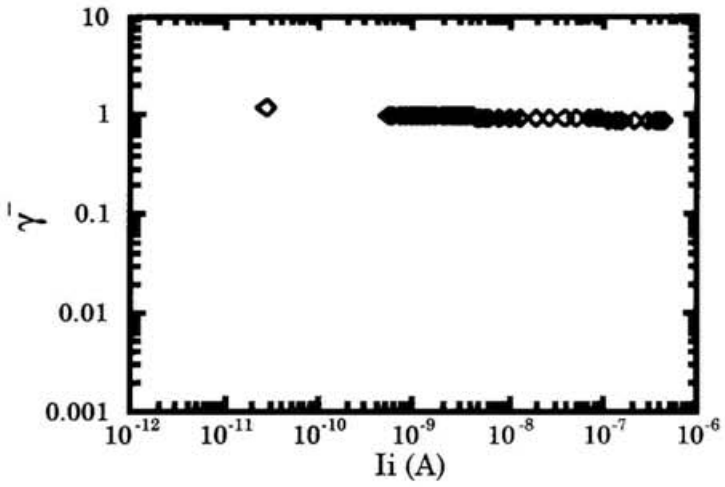

Figure 4-11 Ion-flux dependence of γ^- induced by 2.5 keV H^- impact on $SrCeO_3$ (5 % Yb). No potential is applied to the inner cup.

Figure 4-12 shows a typical Auger electron spectrum from $SrCeO_3$ (5% Yb) surface after 20 minute sputtering by Ar^+ ion at 25 $\mu A/cm^2$. It is noticed that the density of O is low and that of Sr is high, compared with its composition. Figures 4-13 (a) and (b) show the inner cup bias potential dependence of γ induced by 2.5 keV proton impact on unclean $SrCeO_3$ (5% Yb) at low and high fluxes of the incident proton beam, respectively. It is found that γ^- and γ^+ are constant at the bias potential over +50 V and below -50 V, respectively, at low incident beam fluxes (see Fig. 4-13 (a)). But at high fluxes, γ^+ seems to be practically the same as that at low fluxes but no plateau region of γ^- can be observed even at the bias potential of +200 V (see Fig. 4-13 (b)).

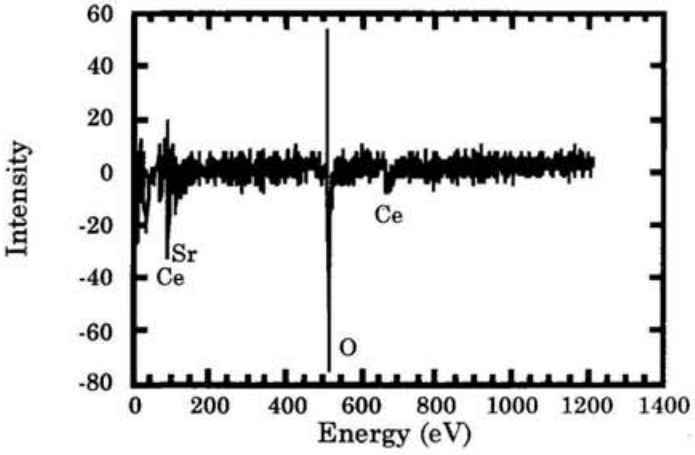

Figure 4-12 A typicalAuger electron spectrum from $SrCeO_3$ (5% Yb) after sputtering by Ar ions. The surface densities of O, Sr and Ce have been estimated to be 18.6, 69.3 and 12.1 %, respectively.

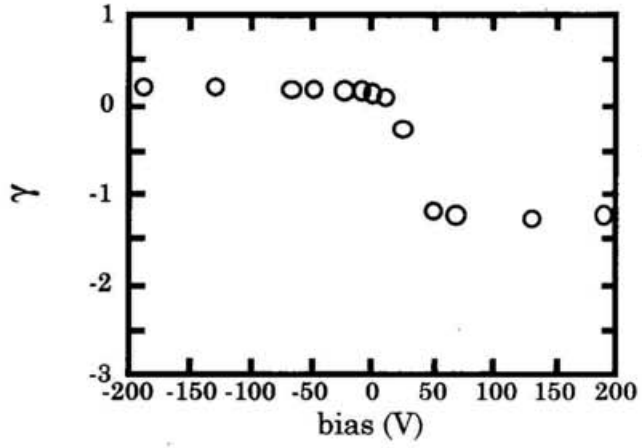

Figure 4-13 (a) Inner cup bias potential dependence of γ for unclean $SrCeO_3$(5% Yb) at low fluxes of 2.5 keV incident proton beam (about 3×10^{-10} A).

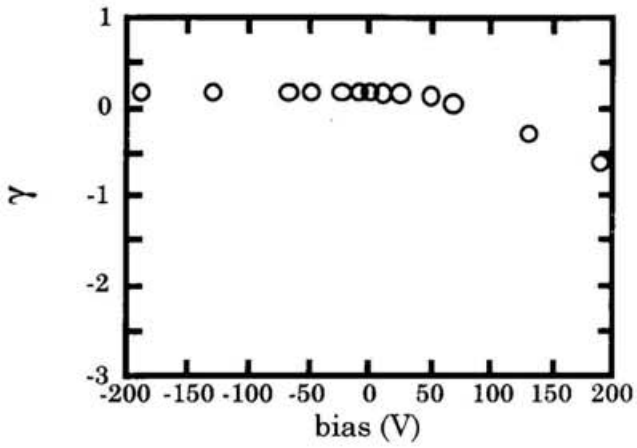

Figure 4-13 (b) Inner cup bias potential dependence of γ for unclean $SrCeO_3$(5% Yb) at high fluxes of 2.5 keV incident proton beam (about 2×10^{-9} A).

References

[BAF 1979] R. A. Baragiola, E. V. Alonso, J. Ferron and A. Oliva-Florio, Surf. Sci. 90 (1979) 240

[T 1995] E. W. Thomas, Report of International Atomic Energy Agency, INDC (NDS)-322 , (IAEA, Vienna, Feb., 1995)

Chapter 5 Experimental results of the mass and energy of secondary ions emitted from surfaces

As described in Chapter 4, a considerable positive ion emission yields were observed. In this chapter, how the positive ions were identified and how the energy of the positive ions was estimated are described.

5-1 Identification of secondary positive ions

Rutherford backscattering spectra (RBS) from graphite and beryllium collectors for $YBa_2Cu_3O_7$ are shown in Figs. 5-1 and 5-2, respectively. In these figures, spectra (a), (b) and (c) correspond to those obtained at 60 keV H_2^+ (total accumulated charge = 0.01 C), 100 keV Ar^+ (0.015 C) ion impact and the unirradiated collectors. From spectra of the particles accumulated on both collectors which are obtained using 100 keV Ar^+ ion (see Figs. 5-1 (b) and 5-2 (b)), the elements composing the target, Y, Ba, Cu and O, are clearly observed. The Ar peak is seen on the beryllium collector, but not on the graphite collector. This is probably due to the different sticking probabilities between beryllium and graphite. In 60 keV H_2^+ impact, it is also recognized that the target elements are deposited on both collectors although the intensities are low.

RBS spectra for graphite and beryllium collectors from $SrCeO_3$ (5 % Yb) target are also shown in Figs. 5-3 and 5-4. Similar to those from $YBa_2Cu_3O_7$, these figures show the spectra (a) under 60 keV H_2^+ (0.03 C) and (b) 100 keV Ar^+ (0.012 C) ion impact, respectively, and (c) the unirradiated collectors. The target elements, Sr, Ce, Yb and O, were also recognized. From the spectra in Figs. 5-3 (b) and 5-4 (b), it is noticed that intensities of target elements are larger for Ar^+ ion impact than for H^+ ion impact, suggesting that these target elements are more sputtered by heavier ion impact, as expected.

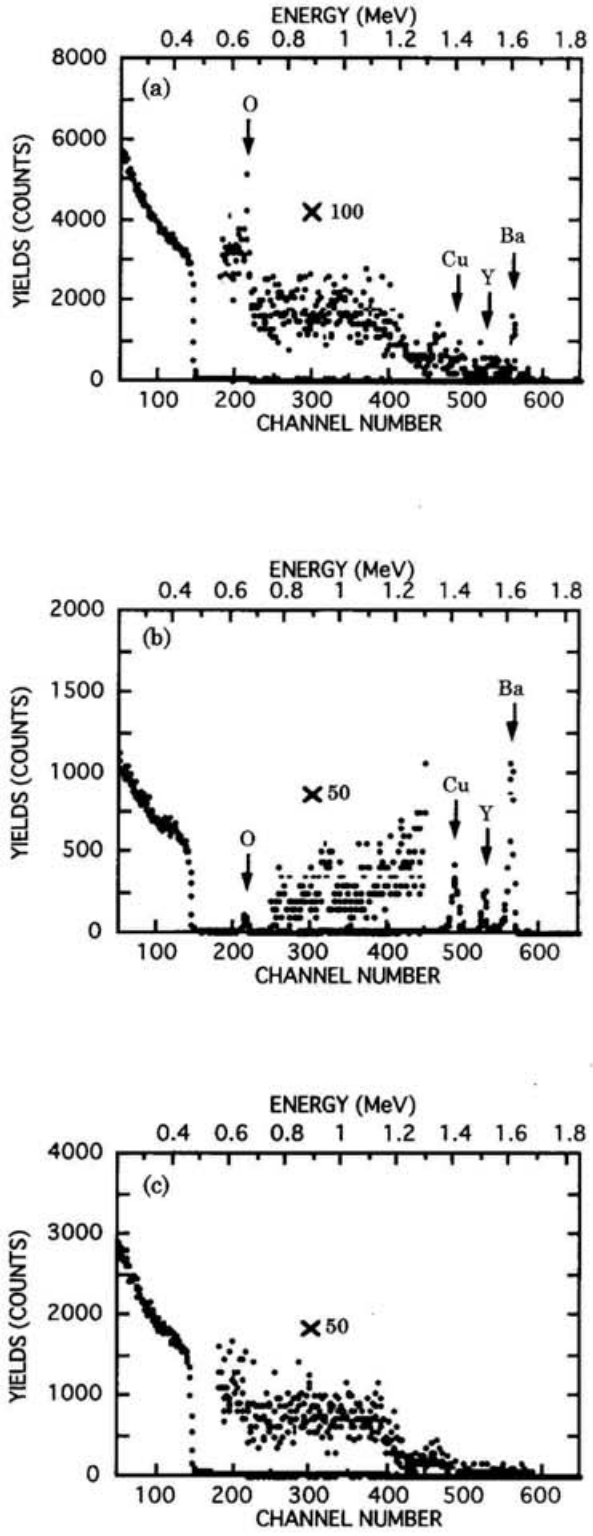

Figure 5-1 RBS spectra of 1.8 MeV He from graphite sheets which collect the secondary ions from $YBa_2Cu_3O_7$: (a) 60 keV H_2^+, (b) 100 keV Ar^+ irradiated and (c) unirradiated graphites.

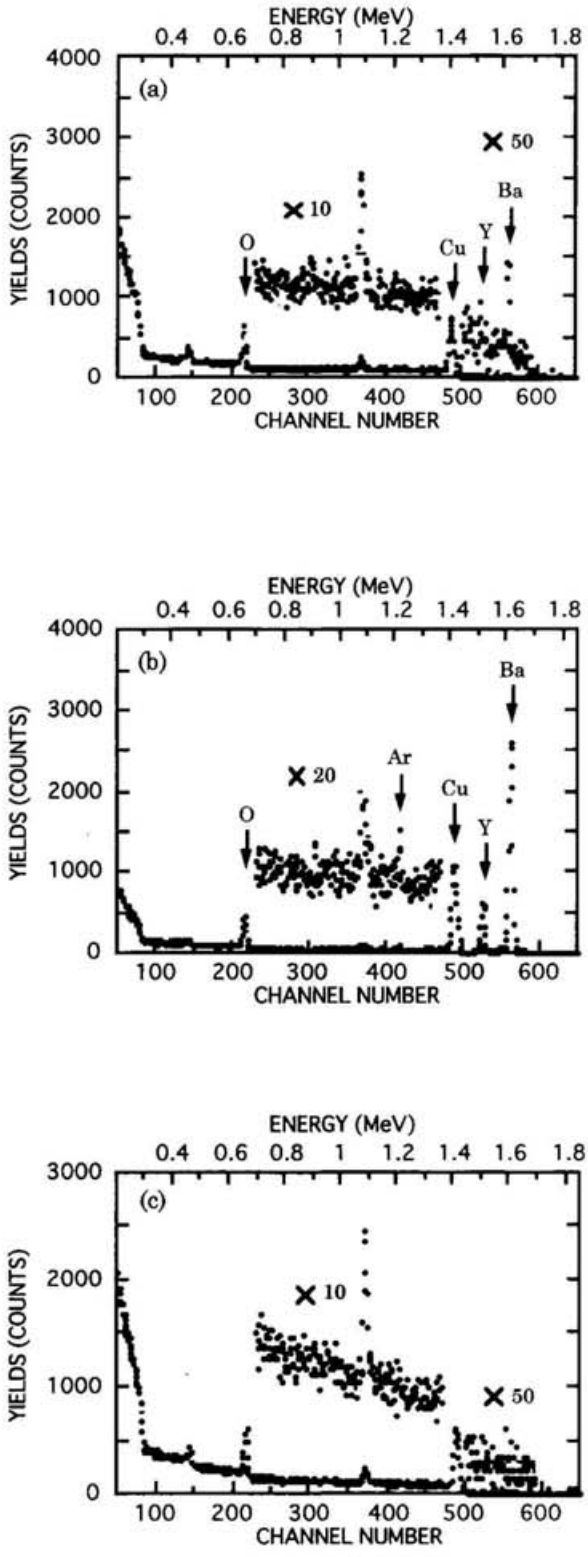

Figure 5-2 RBS spectra of 1.8 MeV He from beryllium sheets which collect the secondary ions from $YBa_2Cu_3O_7$: (a) 60 keV H_2^+, (b) 100 keV Ar^+ irradiated and (c) unirradiated berylliums.

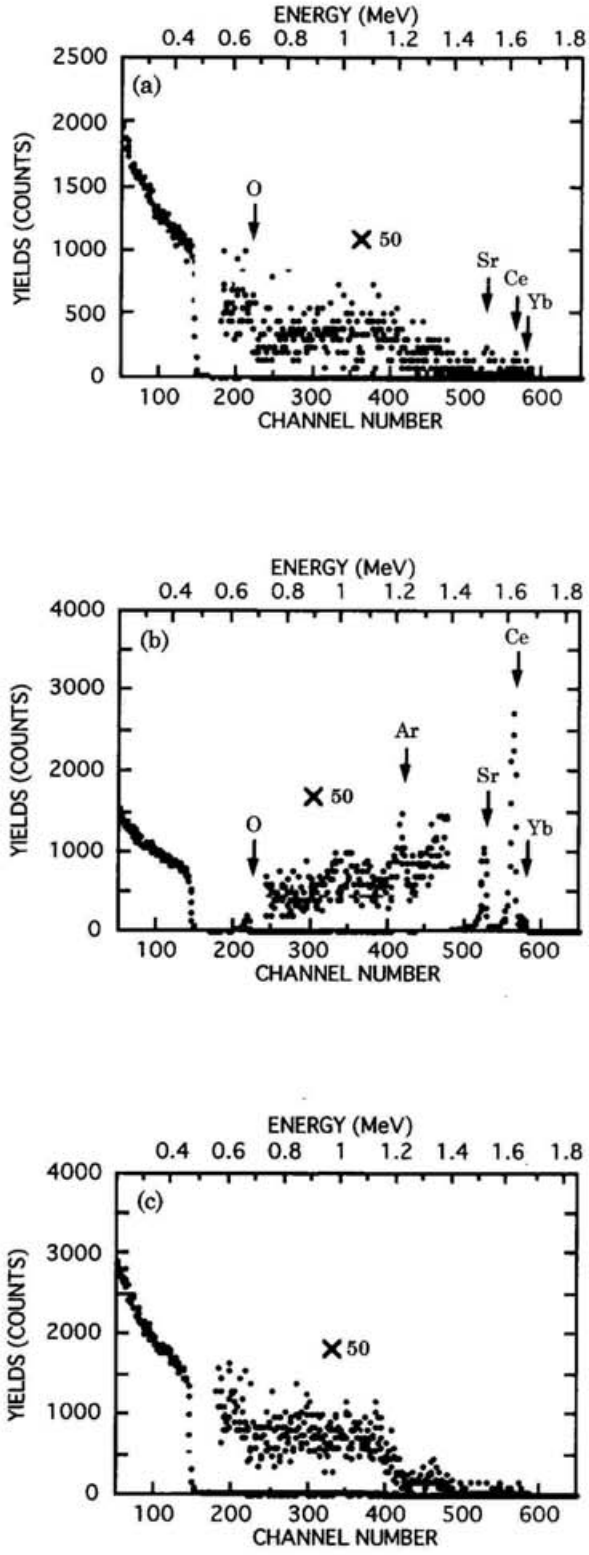

Figure 5-3 RBS spectra of 1.8 MeV He from graphite sheets which collect the secondary ions from $SrCeO_3$ (5 % Yb): (a) 60 keV H_2^+, (b) 100 keV Ar^+ irradiated and (c) unirradiated graphites.

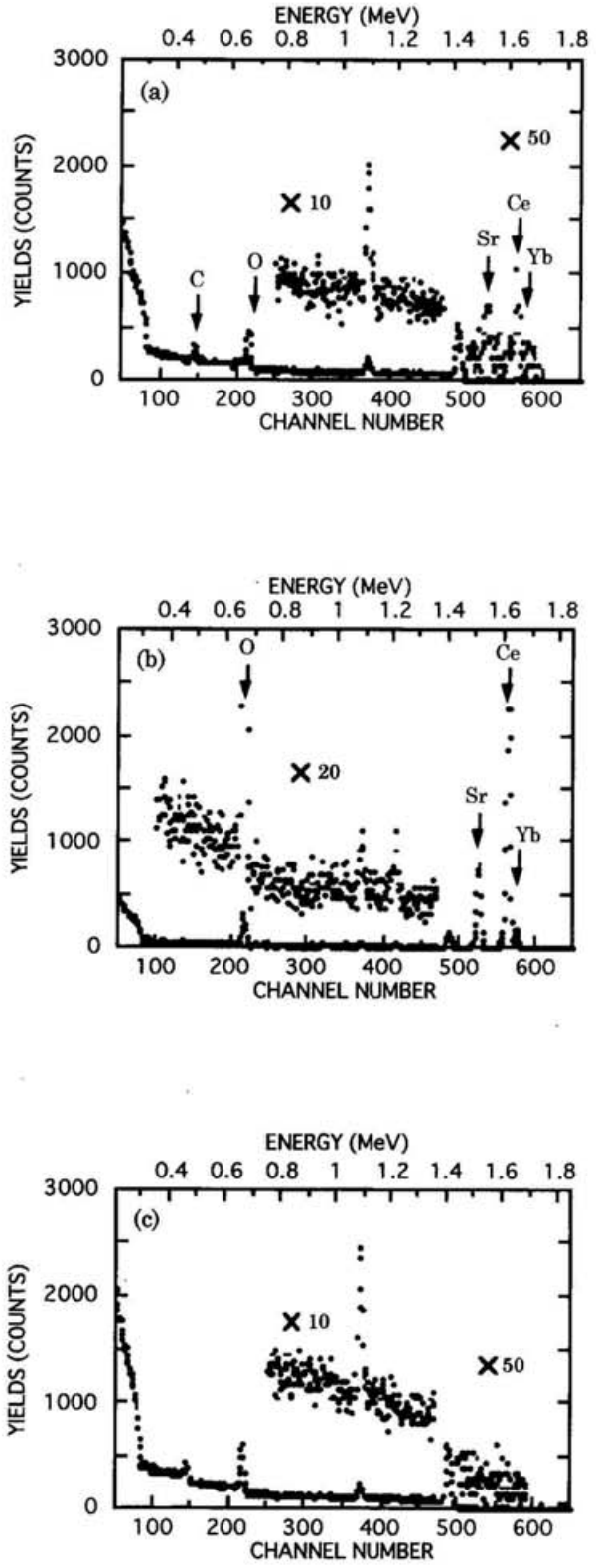

Figure 5-4 RBS spectra of 1.8 MeV He from beryllium sheets which collect the secondary ions from $SrCeO_3$ (5 % Yb): (a) 60 keV H_2^+, (b) 100 keV Ar^+ irradiated and (c) unirradiated berylliums.

5-2 Mass and energy distributions of secondary ions

The observed results of the secondary ion emissions from $SrCeO_3$ (5% Yb) at high incident ion fluxes described in Chapter 4 (see Fig. 4-13 (b)) indicate the emission of high energy positive ions. In this section, the experimental results which are obtained using the retarding technique (see Fig. 3-5 in Chapter 3) are shown.

Figures 5-5 (a)-(c) show the observed ion mass spectra from $SrCeO_3$ (5 % Yb) target impacted by 0.8 keV Ar^+ ions with relatively high current (~460 nA). From these spectra, peaks of singly charged Sr and Ce are recognized. It is important to note that these peaks have been observed, even at the retardation voltage as high as 300 V and 500 V. In Fig. 5-6 is shown the retarding potential dependence of Sr and Ce ion intensities induced by 0.8 keV Ar^+ ions on $SrCeO_3$ (5 % Yb). Each intensity was normalized to the incident Ar^+ ion current. This shows that the secondary positive ions, Sr^+ and Ce^+, should have large kinetic energy, roughly equal to the incident ion energy. Unfortunately no ion mass spectra could be taken at low incident ion current, because the collection efficiencies were too low to detect the secondary ions because of small acceptance angles of the present detection system.

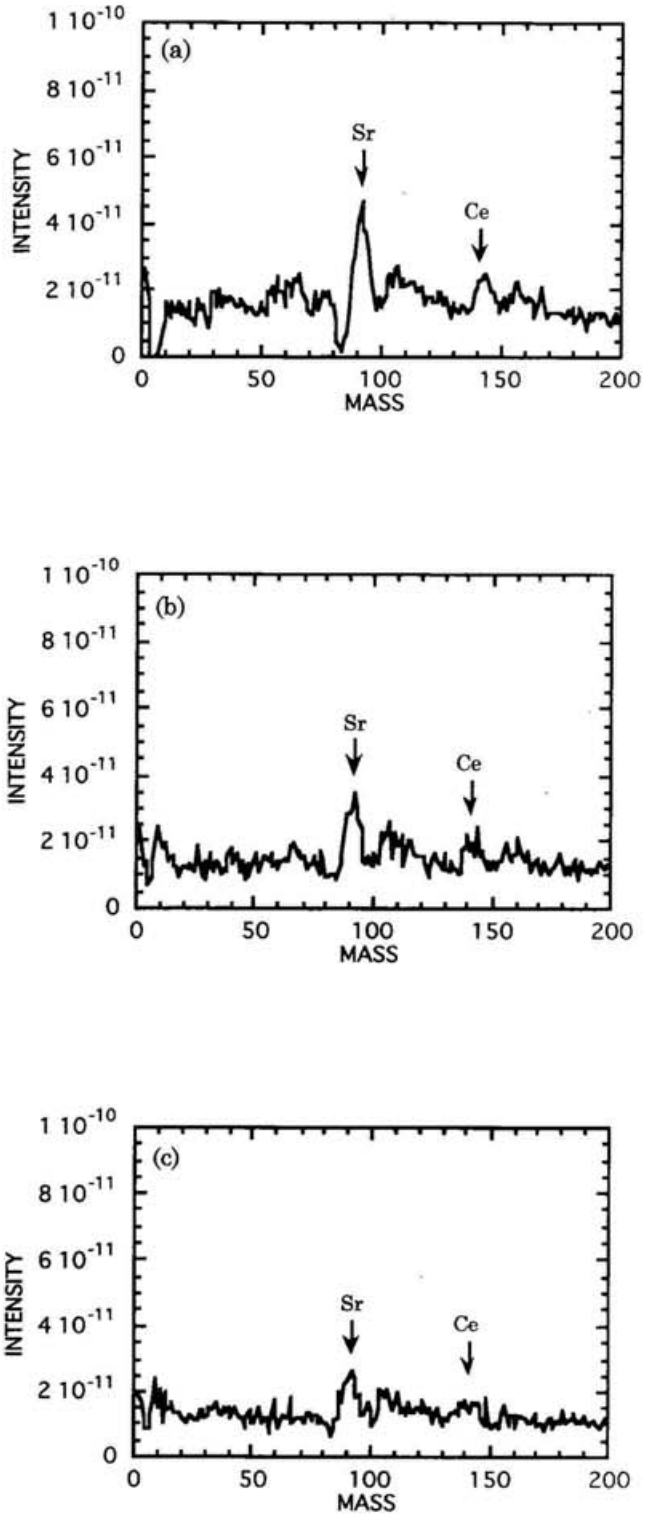

Figure 5-5 Ion-mass spectra from $SrCeO_3$ (5 % Yb) impacted by 0.8 keV Ar^+ ions. The retardation potential of 0, +300 and +500 V was applied for (a), (b) and (c), respectively.

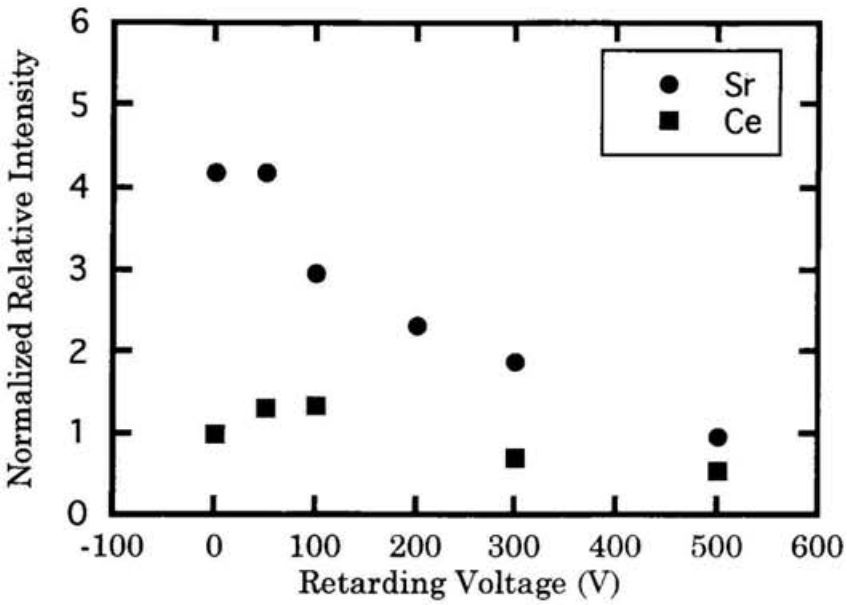

Figure 5-6 Retarding potential dependence of Sr and Ce ions induced by 0.8 keV Ar^+ ions on $SrCeO_3$(5 % Yb).

Chapter 6 Discussion on the observed secondary electron and positive ion emission yields

6-1 The secondary electron emission yields

According to the theories (see eq. 2-6), the secondary electron emission yields due to the kinetic emission are proportional to the electronic stopping power in solids and Λ_- is roughly independent of the incident ion energy. Indeed it has been shown that Λ_- is nearly constant and approximately 0.01 ± 0.003 (nm/eV) for clean Ag, Al, Au and Cu metal targets in a wide range of the proton impact energy, except for very low impact energy (see Appendix 2). However, there is no simple relation between the secondary electron emission yield and the electronic stopping power for heavy projectile impact [H 1991]. At low energy ion impact, in particular, Λ_- strongly depends on the projectile-target combination.

γ^- induced by low energy rare gas ion impact on alkali-halide targets had been observed to have the energy dependence similar to γ^- for metal targets [KKR 1975]. The deduced Λ_- for alkali-halides are shown in Appendix 3. It is found that Λ_- is much larger than those for metal targets and also for the non-metallic targets obtained in the present work (see the detailed discussion later in this section).

Now we would like to discuss the relation between the secondary electron emission yield (γ^-) and the electronic stopping power (S_e) in non-metallic oxides observed in the present work. Figures 6-1 (a) and (b) show the incident energy dependence of γ^- for H^+ and Ar^+ ion impact on $YBa_2Cu_3O_7$, respectively, which is compared with $\Lambda_- S_e$. It should be noted that Li et al. [LKT 1995] had identified the negative secondary ions from $YBa_2Cu_3O_7$ in their SIMS study but not given any quantitative information.

γ^- could deviate from the S_e curve if the negative ions would significantly contribute to γ^- as the negative ion contribution is expected to be proportional to the nuclear stopping power. On the other hand, the observed γ^- curve follows exactly the S_e, indicating that indeed the dominant component of the negative charged particles emitted from surfaces consists of electrons but not any negative ions. The coefficients Λ_- for $YBa_2Cu_3O_7$ under both H^+ and Ar^+ ion impact are found to be larger by a factor of 2-3 than those from clean metal surfaces.

Similarly, Figs. 6-2 (a) and (b) show the incident energy dependence of γ^- for H^+ and Ar^+ ion impact on $SrCeO_3$(5% Yb), respectively. Here, γ^- is taken from the averaged values at low ion current. The observed γ^- is found to follow the S_e curve with constants Λ_-. The coefficient Λ_- for $SrCeO_3$(5% Yb) is also found to be larger by a factor of 2-3 than that of clean metal surfaces.

As mentioned already in γ^--S_e relation in the secondary electron emissions, similar relationship of γ^+ with the nuclear stopping power S_n can be expected to hold, namely $\gamma^+ = \Lambda_+ S_n$ (Λ_+ estimated thus is given in Table 6-3.). Similar dependence of γ^+ and Λ_+ are also shown in Figs. 6-1 (a) and (b) for $YBa_2Cu_3O_7$ and in Figs. 6-2 (a) and (b) for $SrCeO_3$(5% Yb). The detailed discussion of γ^+ will be given in section 6-2.

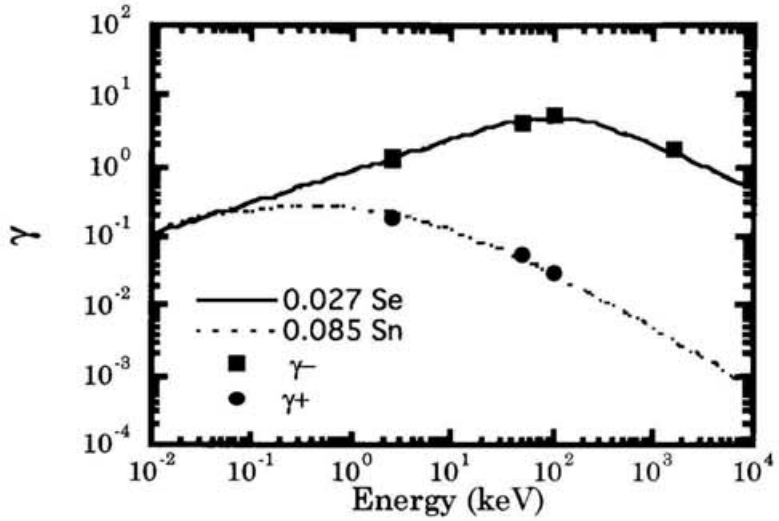

Figure 6-1 (a) The incident energy dependence of γ^- and γ^+ in H^+ impact on $YBa_2Cu_3O_7$. The data of γ^- for 1.6 MeV H^+ are taken from ref. [RLK 1988]. The solid line correspond to the calculated electronic stopping power S_e with constant Λ_-, meanwhile the dotted line correspond to the calculated nuclear stopping power S_n with constant Λ_+.

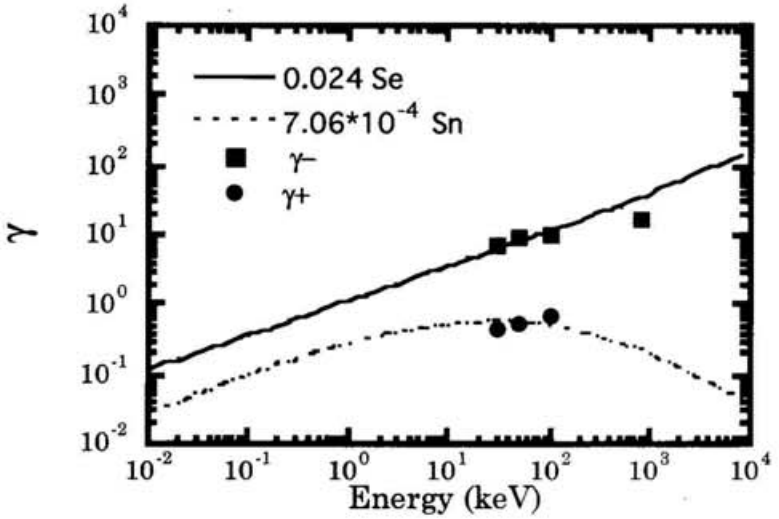

Figure 6-1 (b) The incident energy dependence of γ^- and γ^+ in Ar^+ impact on $YBa_2Cu_3O_7$. The data of γ^- for 800 keV Ar^+ are taken from ref. [RLK 1988]. The solid line correspond to the calculated electronic stopping power S_e with constant Λ_-, meanwhile the dotted line correspond to the calculated nuclear stopping power S_n with constant Λ_+.

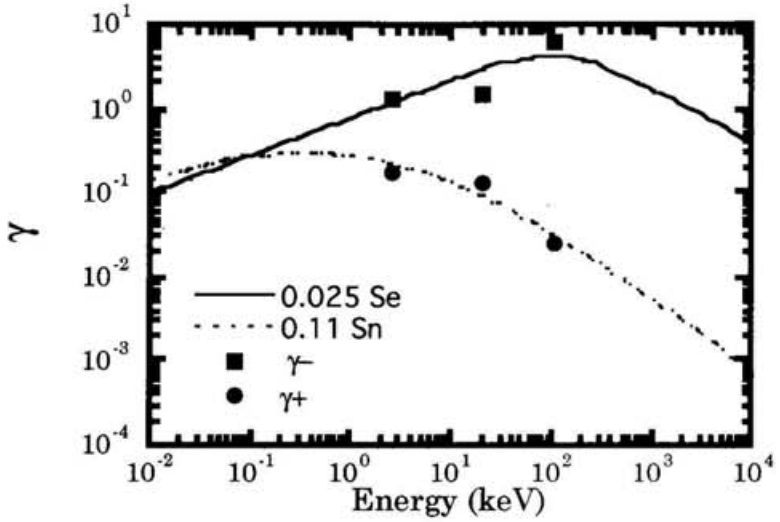

Figure 6-2 (a) The incident energy dependence of γ^- and γ^+ in H^+ impact on $SrCeO_3$(5 % Yb). The solid line correspond to the calculated electronic stopping power S_e with constant Λ_-, meanwhile the dotted line correspond to the calculated nuclear stopping power S_n with constant Λ_+.

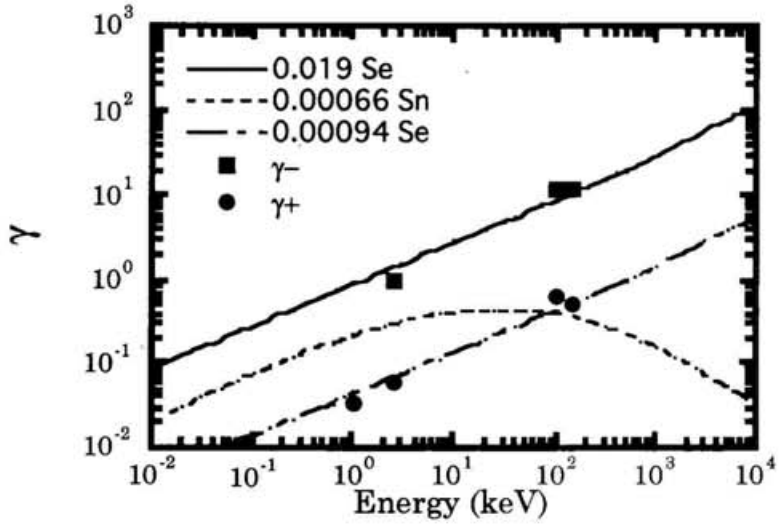

Figure 6-2 (b) The incident energy dependence of γ^- and γ^+ in Ar^+ impact on $SrCeO_3$(5 % Yb). The solid line correspond to the calculated electronic stopping power S_e with constant Λ_-, meanwhile the dotted line correspond to the calculated nuclear stopping power S_n with constant Λ_+. The dash-dotted line corresponds to the electronic stopping power S_e with different constant.

In Tables 6-1 (a) and (b), the observed γ^- and the deduced Λ_- for $YBa_2Cu_3O_7$ and $SrCeO_3$ (5 % Yb) are summarized. As shown in Chapter 4, γ^- for clean TiO_2 is almost the same as that for clean metal targets. On the other hand, that for $YBa_2Cu_3O_7$ and $SrCeO_3$ (5 % Yb) is very large, compared with that for clean metal targets.

Table 6-1 (a) Experimental results of γ^- for $YBa_2Cu_3O_7$. Λ_- is given as $\Lambda_- = \gamma^- / S_e$.

Ion	E(keV)	γ^-	Λ_-
H^+	2.5	1.3	0.024
H^+	50	4.4	0.025
H^+	100	5.5	0.029
Ar^+	30	7.5	0.028
Ar^+	50	9	0.026
Ar^+	100	10	0.020

Table 6-1 (b) Experimental results of γ^- for $SrCeO_3$ (5 % Yb). Λ_- is given as $\Lambda_- = \gamma^- / S_e$.

Ion	E(keV)	γ^-	Λ_-
H^+	2.5	1.3	0.027
H^+	20	1.5	0.012
H^+	100	6	0.035
Ar^+	2.5	1	0.013
Ar^+	100	12	0.025
Ar^+	150	12	0.020

Though the available data of γ^- for non-metallic targets are very limited, the present Λ_- can be compared with other published data and is summarized in Table 6-2.

Table 6-2 Proportional coefficients Λ_- (nm/eV) for various non-metallic targets. Data with asterisks are from the present work. Others are taken from refs. [DS 1975], [SW 1972] and [BMB 1988].

	BeO	TiO_2	Al_2O_3	$SrCeO_3$ (5 % Yb)	$YBa_2Cu_3O_7$
H^+	0.019*		0.027	0.025*	0.027*
Li^+	0.030	0.024	0.023, 0.038		
Na^+	0.032		0.050		
Ar^+				0.019*	0.024*
K^+	0.029		0.034		
Rb^+	0.040		0.041		
Sr^+		0.034	0.027		
Cs^+	0.049	0.037	0.034, 0.049		
Ba^+		0.047	0.038		
Ave.	0.033	0.035	0.036	0.022	0.026

Dietz et al. [DS 1975] : Li^+, Na^+, K^+, Rb^+ and Cs^+ (4-30 keV) + Al_2O_3 and BeO

Stein et al. [SW 1972] : Cs^+, Ba^+, Li^+ and Sr^+ (10-40 keV) + Al_2O_3 and TiO_2

Borovsky et al. [BMB 1988] : H^+ (5-24 MeV) + oxidized aluminum

Note in this table that the present data for TiO_2 targets are not included as they have been obtained only at a single energy.

These results show that the proportional coefficients Λ_- for oxidized surfaces and oxide targets are 0.02-0.05 nm/eV on average, which can be compared with 0.01 nm/eV for metal targets (see Appendix 2).

Among the main mechanisms in the secondary electron emission from solids already described in Chapter 2, the total secondary electron productions under particle impact are known to be not much different in metal and non-metallic

materials. Therefore, the observed difference of Λ_- between metal and non-metallic surfaces can be, at least qualitatively, understood from two other effects:

1) the mean free path of the secondary electrons in solids,

2) the surface barrier potential.

According to Ashley et al. [AA 1981], the inelastic mean free path of electrons in SiO_2 is larger by a factor of 2-10 than that in Si in low energy region (< 100 eV). Similar trend has also been observed in Al_2O_3 and Al [TPP 1988], [A 1988]. Because the average kinetic energy of the secondary electrons produced in solids is low, the mean free path of low energy electrons in oxide materials can be assumed to be larger than that for metals. In turn, this difference should have significant influence upon the transfer of the free electrons toward the solid surfaces.

It is well known that the surface barrier potential is significantly changed by the adsorption of other particles on the surfaces. Generally, the surface barrier potential of oxide targets is small, compared with that in metals. Thus, two effects combined, namely the increased mean-free path and the reduced work function, are expected to enhance the secondary electron yields for the oxides and oxygen covered surfaces.

In fact, as Köning et al. [KKR 1975] had shown, the energy of the maximum intensity of the secondary electrons emitted from alkali-halide targets shifts toward lower energy, compared with that from metals. The shift is believed to result from the combined effects of the increased mean-free path for low energy electrons and the reduced surface barrier potential.

6-2 The secondary positive ion emission yields

Tables 6-3 (a)-(e) summarize γ^+ observed in the present study as well as the total sputtered yields Y_s and the total backscattered particle yields Y_b. In these tables, the published experimental data or the deduced values from a semi-empirical formula are used for Y_s and Y_b. And, if neither experimental data nor semi-empirical formulas are found, the results calculated by TRIM code [ZBL 1985] are used. It should be noted that, generally, the charged fractions in the sputtered and backscattered particles are very small and at best a few % at the present energy region.

On the other hand, Y_c is the secondary electron emission yield from the inner surface of the inner cup made of stainless steel under the backscattered neutral particle bombardment (see the detail later in this section) which is estimated in the present analysis.

Table 6-3 (a) Comparison of the observed γ^+ with total backscattered yields Y_b and total sputtered yields Y_s for clean Cu. Data point with superscript 0) is deduced from a semi empirical formula and that with superscript 1) is the experimental results. Other data for Y_s and Y_b are calculated by TRIM code. Y_c is the estimated secondary electron emission yield from the inner surface of the inner cup made of stainless steel under the backscattered neutral particle bombardment. Λ_+ is the ratio of γ^+ to the nuclear stopping power S_n.

Ion	E(keV)	γ^+	Y_b	Y_s	Y_c	Λ_+
H^+	2.5	0.18	0.18 [0)]	0.050	0.15	0.055
Ar^+	2.5	7.6×10^{-4}	0.057	4.6 [1)]	5.6×10^{-4}	7.7×10^{-4}

0) Ito et al. [ITI 1985]

1) Southern et al. [SWR 1963]

Table 6-3 (b) Comparison of the observed γ^+ with total backscattered yields Y_b and total sputtered yields Y_s for clean Be. Data point with superscript 0) is deduced from a semi empirical formula and that with superscript 1) is the experimental result. Y_c is the estimated secondary electron emission yield from the inner surface of the inner cup made of stainless steel under the backscattered neutral particle bombardment. Λ_+ is the ratio of γ^+ to the nuclear stopping power S_n.

Ion	E(keV)	γ^+	Y_b	Y_s	Y_c	Λ_+
H^+	2.5	0.027	0.025 [0)]	0.013 [1)]	0.013	0.011

0) Ito et al. [ITI 1985]

1) Roth et al. [RBO 1979]

Table 6-3 (c) Comparison of the observed γ^+ with TRIM calculation for clean TiO_2. Y_b and Y_s are total backscattered and sputtered particle yields calculated by TRIM code, respectively. Y_c is the estimated secondary electron emission yield from the inner surface of the inner cup made of stainless steel under the backscattered neutral particle bombardment. Λ_+ is the ratio of γ^+ to the nuclear stopping power S_n.

Ion	E(keV)	γ^+	Y_b	Y_s	Y_c	Λ_+
H^+	2.5	0.13	0.053	8.4×10^{-3}	0.032	0.040
Ar^+	2.5	0.092	6.3×10^{-3}	0.79	2.0×10^{-5}	1.3×10^{-4}

Table 6-3 (d) Comparison of the observed γ^+ with TRIM calculation for $YBa_2Cu_3O_7$. Y_b and Y_s are total backscattered and sputtered particle yields calculated by TRIM code, respectively. Y_c is the estimated secondary electron emission yield from the inner surface of the inner cup made of stainless steel under the backscattered neutral particle bombardment. Λ_+ is the ratio of γ^+ to the nuclear stopping power S_n.

Ion	E(keV)	γ^+	Y_b	Y_s	Y_c	Λ_+
H^+	2.5	0.18	0.088	0.023	0.062	0.071
H^+	50	0.056	5.7×10^{-3}	1.4×10^{-3}	0.019	0.099
H^+	100	0.03	2.3×10^{-3}	6.9×10^{-4}	0.010	0.086
Ar^+	30	0.47	0.031	3.2	0.013	5.5×10^{-4}
Ar^+	50	0.52	0.025	2.9	0.020	6.3×10^{-4}
Ar^+	100	0.7	0.019	2.4	0.031	9.4×10^{-4}

Table 6-3 (e) Comparison of the observed γ^+ with TRIM calculation for $SrCeO_3$(5% Yb). Y_b and Y_s are total backscattered and sputtered particle yields calculated by TRIM code, respectively. Y_c is the estimated secondary electron emission yield from the inner surface of the inner cup made of stainless steel under the backscattered neutral particle bombardment. Λ_+ is the ratio of γ^+ to the nuclear stopping power S_n.

Ion	E(keV)	γ^+	Y_b	Y_s	Y_c	Λ_+
H^+	2.5	0.18	0.078	4.6×10^{-3}	0.059	0.087
H^+	20	0.13	0.018	2.0×10^{-3}	0.040	0.15
H^+	100	0.025	2.6×10^{-3}	2.1×10^{-4}	0.011	0.084
Ar^+	1.0	0.035	0.077	0.84	4.7×10^{-4}	1.0×10^{-4}
Ar^+	2.5	0.063	0.062	1.2	1.2×10^{-3}	1.4×10^{-4}
Ar^+	100	0.65	0.027	1.3	0.043	1.5×10^{-3}
Ar^+	150	0.5	0.020	1.1	0.045	8.9×10^{-4}

When a cup is used in order to collect the emitted charged particles from a target, we need to know the contribution of the secondary electron emission yields from the inner surfaces of the inner cup made of stainless steel bombarded by neutral particles which are backscattered from the target, namely the sputtered and backscattered neutral particles. As the negative potential has been applied to the inner cup when γ^+ is measured, these secondary electrons from the inner surface can leave the inner cup and reach the target (see Fig. 6-3 (a)). Apparently these secondary electrons increase the observed γ^+. On the other hand, when γ^- is measured with the positive potential applied on the inner cup, these secondary electrons can not leave the inner cup surfaces (see Fig. 6-3 (b)) and do not influence the measured γ^-.

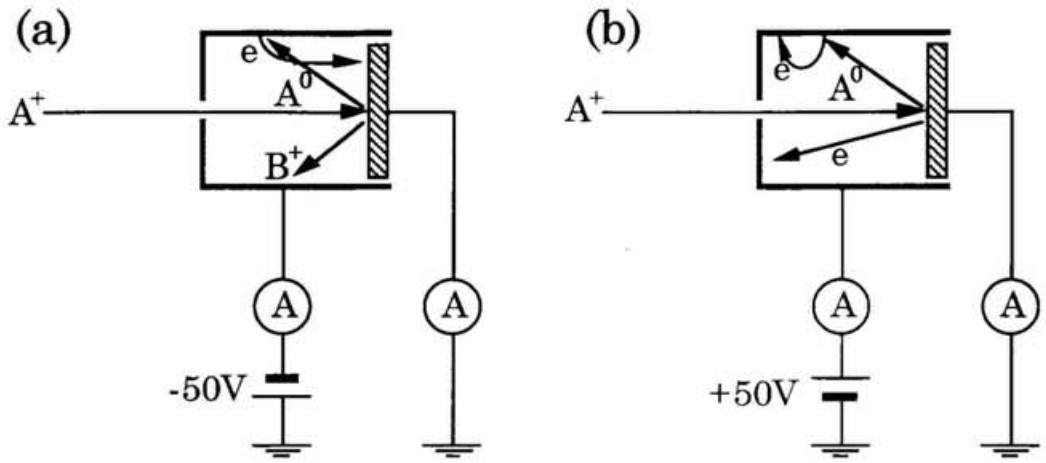

Figure 6-3 The effect of the secondary electron emission from the walls of the inner cup induced by the backscattered neutral particles. (a) : the negative bias potential is applied to the cup to measure γ^+. (b) : the positive bias potential is applied to the cup to measure γ^-.

The results calculated by TRIM code indicate that most of the sputtered particles have the kinetic energy less than 100 eV. Therefore we can discard the secondary electron emissions induced by impact of these sputtered particles on the stainless steel surface. On the other hand, the contribution of the backscattered neutral particles can not be neglected as they may have the kinetic energy sufficient to kick out the secondary electrons. In order to estimate the contribution of the backscattered neutral particles, we need the following procedures.

Using the TRIM code, the number, energy and angle of the backscattered atoms have been calculated. Using the formula for γ^- as a function of the incident energy at normal incidence and the normalized electron yield as a function of the incident angles (see Appendix 4), we can estimate the emitted electrons from the inner wall of the inner cup induced by the backscattered atoms as given as Y_c in Tables 6-3 (a)-(e).

In Tables 6-3 (a) and (b), it is noticed that the calculated Y_c is nearly the same as the observed γ^+ for clean Cu and Be targets. This shows that most of the observed γ^+ for clean Cu and Be are the contribution of the secondary electrons

from the inner cup. However, the present γ^+ for $SrCeO_3$ (5 % Yb) and $YBa_2Cu_3O_7$ is clearly far larger than that for metal targets even if the contribution of the secondary electrons from the inner wall of the cup induced by the backscattered neutral particle impact (Y_c in Tables 6-3 (a)-(e)) is taken into consideration.

Especially, for H^+ impact, the secondary positive ion emission yields γ^+ are much larger than total sputtering yields calculated by TRIM code. But it is difficult to discuss absolute values of the secondary positive ion emission yields γ^+ for H^+ ion impact, since the contribution of Y_c can not be neglected. On the other hand, it is possible to discuss the incident energy dependence of γ^+ under Ar^+ ion impact on oxide surfaces, because Y_c for Ar^+ ion impact is sufficiently small. If these secondary ions emitted from oxide surfaces were a part of the sputtered particles induced by kinetic energy of incident ions, γ^+ would be expected to be proportional to S_n. However, as shown in Fig. 6-2 (b), it has been found that the observed γ^+ induced by Ar^+ ion impact on $SrCeO_3$ (5% Yb) is proportional not to S_n (see the dotted curve in Fig. 6-2 (b)), but more likely to S_e (see the dash-dotted curve in Fig. 6-2 (b)). This result provides the important consequence in the secondary ion emissions from the non-metallic surfaces under low energy positive ion impact as follows:

The present experimental results clearly indicate that these secondary ions emitted from $SrCeO_3$ (5% Yb) are target elements ionized through interactions with the incident positive ions. Among various interactions between the incident ion and the target at low impact energy used in the present work, the electron transfer from the target into the incident ions is likely the most dominant mechanism for the secondary ion productions from the non-metallic targets, though the direct ionization of the target can become important at higher energies. Indeed the cross sections for the electron transfer is expected to increase slowly as the incident ion energy increases, in agreement with the observed γ^+ behavior in the present work (see Fig. 6-2 (b)). These positive ions formed and accumulated on non-metallic surfaces with high electric resistivities interact repulsively with each other (This is often called the Coulomb explosion.). Then, a part of these ions

after over coming the surface barriers can escape from the surfaces into vacuum.

Furthermore, the present mass and energy analysis of the secondary ions emitted from these oxide targets indicate that the target component ions are emitted and have large kinetic energies for $SrCeO_3$ (5 % Yb). It is clear that the mechanisms of secondary positive ion emissions from these targets are different from *physical sputtering* induced by the kinetic energy of the incident ions.

For $SrCeO_3$ (5 % Yb) which have large electric resistivity, similar to insulators, the accumulation of the incident ion charge on the surfaces should be taken into account. The observed large positive ion yields at high incident ion fluxes for $SrCeO_3$ (5 % Yb) with +50 V bias potential at the inner cup can be understood as follows: If, as a consequence of the charge-accumulation, the charge-accumulated voltage on the target surfaces becomes higher than the potential applied to the inner cup, the secondary electrons emitted from the wall of the inner cup are accelerated toward the target and, as a result, the measured γ^+ becomes apparently large. On the other hand, this charge-accumulated voltage on the target surfaces, in particular at high fluxes, can accelerate the secondary ions emitted from the target and provide the kinetic energy to the secondary ions which can be as large as the incident ion energy.

Also such charge-accumulation on the surfaces can cause the break-up of the surface structures induced by the Coulomb repulsive force, because charged particles which have been ionized by direct ionizations or electron transfers in nearly the target surface by incident ions can not be neutralized smoothly due to the large electric resistivity of these targets. Recently the Coulomb explosion has been studied by several groups. Cheng et al. [CG 1997-a], [CG 1997-b] investigated the Coulomb explosion using large scale molecular dynamics simulations for Si surfaces and showed that about 10 % of all the ejected particles are ions. Parks et al. [PSB 1997] had investigated the damage caused by impact of low energy, highly charged ions on the insulating surfaces and observed directly the surface topography with nanometer resolutions using an atomic force microscopy (AFM). In that study, they had shown that the volume of damage hillocks on mica as measured by AFM increases as the potential energy

of the incident ions increases. Furthermore, Neidhart et al. [NPA 1995] and Schneider et al. [SB 1996] had measured total sputtered yields induced by highly charged Ar ion impact on LiF and positive ion yields induced by highly charged Kr, Xe and Th ion impact on SiO_2, respectively. From these experimental results, we can extrapolate the secondary positive ion yields which are induced by singly charged projectile ions used in the present studies. The extrapolation of their results to the singly charged ions results in the following secondary ion yields due to the Coulomb explosion: 0.025, 0.023 and 0.026 with the uncertainties of roughly ± 50 % for 2.5 keV H_2^+, H^+ and Ar^+ impact, respectively, for $SrCeO_3$ (5 % Yb).

Table 6-4 The measured γ^+ and various contributions to γ^+ estimated for $SrCeO_3$(5 % Yb) under H_2^+, H^+ and Ar^+ ion impact.

	H_2^+ (2.5 keV)	H^+ (2.5 keV)	Ar^+ (2.5 keV)
γ^+ (measured in this study)	0.31	0.18	0.06
relative	1.72	1	0.33
ion component of sputtered particles	$\sim 10^{-4}$	$\sim 10^{-4}$	$\sim 10^{-3}$
ion component of backscattered particles	$\sim 10^{-3}$	$\sim 10^{-3}$	$\sim 10^{-4}$
secondary electrons due to backscattered neutral particles	0.12	0.059	1.2×10^{-3}
ion component due to Coulomb explosion	0.025	0.023	0.026
Sum	0.15	0.082	0.027
relative	1.83	1	0.33

On the other hand, the positive ion fractions of the sputtered and backscattered particles are considered to be small in this energy region. In Table 6-4 we summarize various contributions to γ^+ for $SrCeO_3$ (5 % Yb).

As mentioned above, however, the contribution of the secondary electrons from the wall of the inner cup induced by the backscattered neutral particle impact is found to be relatively large in the measured γ^+ for H^+ and H_2^+ ion impact but is still too small by more than one order of magnitude in Ar^+ ion impact. Though there are some uncertainties in absolute values in Ar^+ ion impact, significant contribution indeed comes from the ions formed through the Coulomb explosion of the target surfaces. Though the sum of all the contributions is not in good agreement with the observed γ^+, relative intensities among different particle (H_2^+, H^+, Ar^+) impact seem to be in fair agreement with each other (see Table 6-4).

This suggests that such Coulomb explosion on the surfaces seems to play a role in the secondary ion emission from the non-metallic surfaces. Furthermore the local charge-accumulation on the surfaces due to the incident ions is expected to reduce γ^- as the electrons transferred to the solid surfaces can not overcome the potential barrier at the surfaces. Therefore, the dependence of γ for $SrCeO_3$ (5% Yb) on the inner cup bias potential as shown in Figs. 4-13 (a) and (b) can be understood as follows: though +50 V applied to the inner cup is sufficient to collect the secondary electrons at low ion flux region, even +200 V can not bring out the secondary electrons at high ion flux region when the potential barrier at the surface due to the charge-accumulation is formed. On the other hand, the charge-accumulated potential can accelerates ions produced on the surfaces, resulting in production of high energy ions.

References

[A 1988] J. C. Ashley, J. Electron Spectroscopy and Related Phenomena 46 (1988) 199

[AA 1981] J. C. Ashley and V. E. Anderson, J. Electron Spectroscopy and Related Phenomena 24 (1981) 127

[B 1975] A. Benninghoven, Surf. Sci. 53 (1975) 596

[BAO 1979] R. A. Baragiola, E. V. Alonso and A. Oliva-Florio, Phys. Rev. B 19

(1979) 121

[BMB 1988] J. E. Borovsky, D. J. McComas and B. L. Barraclough, Nucl. Instr. Meth. B30 (1988) 191

[CG 1997-a] H. Cheng and J. D. Gillaspy, Application of Accelerators in Research and Industry, edited by J. L. Duggan and I. L. Morgan (1997) 197

[CG 1997-b] H. Cheng and J. D. Gillaspy, Phys. Rev. B 55 (1997) 2628

[DS 1975] L. A. Dietz and J. C. Sheffield, J. Appl. Phys. 46 (1975) 4361

[H 1991] D. Hasselkamp, *Particle Induced Electron Emission* II (Eds. G. Höhler and E. A. Niekisch, Springer-Verlag, Berlin, Heidelberg), Springer Tracts in Modern Physics 123 (1991) 1

[ITI 1985] R. Ito, T. Tabata, N. Itoh, K. Morita, T. Kato and H. Tawara, IPPJ-AM-41 (Institute of Plasma Physics, Nagoya University, 1985)

[KKR 1975] W. Köning, K. H. Krebs and S. Rogaschewski, Int. J. Mass Spectrom. Ion Phys. 16 (1975) 243

[LKT 1995] Yupu Li, J. A. Kilner, T. J. Tate, M. J. Lee, Y. H. Li and P. G. Quincey, Nucl. Instr. Meth. B 99 (1995) 627

[NPA 1995] T. Neidhart, F. Pichler, F. Aumayr, HP. Winter, M. Schmid and P. Varga, Phys. Rev. Lett. 74 (1995) 5280

[PSB 1997] D. C. Parks, M. P. Stöckli, E. W. Bell, L. P. Ratliff, R. W. Schmieder, F. G. Serpa and J. D. Gillaspy, Nucl. Instr. Meth. B (1997 accepted)

[RBO 1979] J. Roth, J. Bohdansky and W. Ottenberger, IPP 9/26 (Inst. Plasma Physics, Garching, Germany, 1979)

[RLK 1988] H. Rothard, P. Lorenzen, N. Keller, O. Heil, D. Hofmann, J. Kemmler, K. Kroneberger, S. Lencinas, K. O. Groeneveld, Phys. Rev. B 38 (1988) 9224

[SB 1996] D. H. G. Schneider and M. A. Briere, Phys. Scrip. 53 (1996) 228

[SW 1972] J. D. Stein and F. A. White, J. Appl. Phys. 43 (1972) 2617

[SWR 1963] A. L. Southern, W. R. Willis and M. T. Robinson, J. Appl. Phys. 34 (1963) 153

[TPP 1988] S. Tanuma, C. J. Powell and D. R. Penn, Surface and Interface Analysis 11 (1988) 577

[ZBL 1985] J. F. Ziegler, J. P. Biersack, U. Littmark, *The Stopping and Ranges of Ions in Solids* (Pergamon Press, Oxford, 1985)

Chapter 7 Concluding remarks and perspectives

In the present study, the secondary charged particles emitted from non-metallic targets have been measured using an ultra high vacuum (~ 10^{-11} Torr) system accompanied with Ar sputtering apparatus in order to understand the interaction mechanisms between low energy ions and non-metallic surfaces.

It is shown that negative charged particle (mostly secondary electron) emission yield γ^- from Be surface strongly depends upon surface oxidation and γ^- for clean Be is about one fifth of that for oxidized Be surface. Similarly, γ^- for unclean TiO_2 is about 3 times larger than that for clean TiO_2. On the other hand, practically no such difference of γ^- has been observed in $YBa_2Cu_3O_7$ and $SrCeO_3$ (5 % Yb) surfaces.

It is also shown that the observed γ^- for $YBa_2Cu_3O_7$ and $SrCeO_3$ (5 % Yb) is large, compared with that for clean metals, and is proportional to the electronic stopping power, similar to the observation in metal targets. The proportional coefficients Λ_- for $YBa_2Cu_3O_7$ and $SrCeO_3$ (5 % Yb) are 0.02~0.03 nm/eV which are nearly equal to those in other oxides observed previously but about 2~3 times larger than those for clean metal targets. Such a difference of the coefficients Λ_- between metal and non-metallic surfaces can be qualitatively explained to be largely due to the difference of the mean free path of the secondary electrons. We have also observed, for the first time, an interesting phenomenon where the observed γ^- for $SrCeO_3$ (5 % Yb) strongly depends on the incident ion flux and becomes to zero above a critical ion flux. It is understood that these phenomena are induced by the local charge-accumulation on the non-metallic surfaces.

The observed positive ion emission yields γ^+ for proton impact are found to be proportional to the nuclear stopping power but a large part of the observed γ^+ are estimated from TRIM code calculations to be due to the secondary electron

emissions from the inner wall of the inner cup induced by the backscattered neutral hydrogen atom impact. On the other hand, the observed γ^+ from $SrCeO_3$ (5 % Yb) surface with Ar^+ ion impact is found to be not related to the nuclear stopping power and is much larger, compared with that for metal targets as well as with that estimated by TRIM code. This enhanced γ^+ is believed to be due to the charged particles produced through the Coulomb explosion on the surfaces of this target, which has relatively high resistivity.

Furthermore, the mass and the energy of the secondary positive charged particles from $YBa_2Cu_3O_7$ and $SrCeO_3$ (5 % Yb) have been measured using two different techniques: 1) the collector method by graphite and beryllium sheets which are analyzed with Rutherford backscattering technique and 2) the quadrupole mass spectrometer with the retarding meshes. In both methods have been observed the ions composing of the targets. Then, it is shown that these secondary ions for $SrCeO_3$ (5 % Yb) are emitted from the surfaces with large kinetic energies, which are provided by the local charge-accumulation of the incident ions on this particular non-metallic target surface at high incident ion fluxes.

It is concluded from the present work that the mechanisms of the secondary charged particle emissions from non-metallic targets are, qualitatively as well as quantitatively, very different from those for metal targets.

A few words should be mentioned on the perspective to pursue the impact of the ions, in particular of highly charged ions which have large potential energy, onto non-metallic as well as insulating materials.

Some interesting topics to be studied are as follows:

1) The secondary electron emissions induced by highly charged ion impact from various non-metallic targets including $SrCeO_3$ (5% Yb) and $YBa_2Cu_3O_7$ as well as the oxide and oxygen-covered targets: In particular, the potential emission can be observed clearly using low kinetic energy, highly charged ions.

2) The yields and the kinetic energy distributions of positive and negative ions emitted from non-metallic targets as well as insulators and the frozen gas targets, which have low binding energy, under impact of highly charged ions: It is

expected that the secondary ion emission yields increase and the secondary ions emitted from target may have large kinetic energy because of the Coulomb explosion.

There are also important applications of such ion-non-metallic material collisions:

1) The sputtering phenomena induced by the potential energy of highly charged ions, which does not give much damage due to the cascade effects in the solids but can be used for controlling the outermost surface layers in VLSI.

2) The sputtering by negative ions where the charge-accumulation on insulating materials is expected to be small.

Appendix 1. The secondary positive ion emission yields for metal targets

The secondary positive ion emission yields γ^+ from clean and oxygen-covered metal surfaces under 3 keV Ar^+ bombardment are summarized in Table A1-1. In this table, sputtering yields Y_s are obtained from calculations by TRIM code and experimental data [1)~5)].

References

[B 1975] A. Benninghoven, Surf. Sci. 53 (1975) 596

[CWC 1977] J. W. Coburn, H. F. Winters and T. J. Chuang, J. Appl. Phys. 48 (1977) 3532

[K 1968] O. K. Kurbatov, Soviet Phys.-Tech. Phys. 12 (1968) 1328

[KRS 1969] V. K. Koshkin, J. A. Rysov, I. I. Shkarban and B. M. Gourmin, Proc. 9th Int. Conf. Phenomena Ionized Gases, Bucharest (1969) p92

[KSO 1979] S. T. Kang, R. Shimizu and T. Okutani, Jpn. J. Appl. Phys. 18 (1979) 1717

[SWR 1963] A. L. Southern, W. R. Willis and M. T. Robinson, J. Appl. Phys. 34 (1963) 153

Table A1-1 Secondary positive ion emission yields from clean and oxygen-covered surfaces under 3 keV Ar^+ bombardment [B 1975].

Metal	γ^+ for clean surface	γ^+ for oxygen-covered surface	Sputtering yield Y_s	γ^+/Y_s for clean surface	γ^+/Y_s for oxygen-covered surface
Al	0.007	0.7	2.4	2.9×10^{-3}	0.29
Ba	0.0002	0.03			
Cr	0.0012	1.2	3.0	4×10^{-4}	0.4
Cu	0.0003	0.007	4.0	7.5×10^{-5}	1.75×10^{-3}
			5.1 [1]		
			4.5 [2]		
Fe	0.0015	0.35	2.6	5.8×10^{-4}	0.135
			2.1 [2]		
Ge	0.0044	0.02	2.5	1.8×10^{-3}	8×10^{-3}
Mg	0.01	0.9			
Mn	0.0006	0.3			
Mo	0.00065	0.4	1.4	4.6×10^{-4}	0.29
			1.6 [2]		
Nb	0.0006	0.05	1.5	4×10^{-4}	0.033
			1.7 [2]		
Ni	0.0006	0.045	2.6	2.3×10^{-4}	0.017
Si	0.0084	0.58	1.2	7×10^{-3}	0.48
			0.96 [3]		
			1.2 [4]		
Sr	0.0002	0.16			
Ta	0.00007	0.02	1.1	6.4×10^{-5}	0.018
Ti	0.0013	0.4	1.1	1.2×10^{-3}	0.36
			1.2 [5]		
V	0.001	0.3	1.6	6.3×10^{-4}	0.19
W	0.00009	0.035	1.4	6.4×10^{-5}	0.025

1) Southern, Willis and Robinson [SWR 1963]

2) Koshkin, Rysov and Shkarban [KRS 1969]

3) Coburn, Winters and Chuang [CWC 1977]

4) Kang, Shimizu and Okutani [KSO 1979]

5) Kurbatov [K 1968]

Appendix 2. The secondary electron emission yields for clean metal targets

Figures A2-1, -2, -3 and -4 show the incident energy dependence of γ^- induced by proton impact on clean Ag, Al, Au and Cu targets, respectively. In these figures, the solid lines represent $\Lambda_- S_e$, where the averaged Λ_- are used for the respective metal targets. In the classical theories, it is expected that the secondary electron emission yield γ^- is proportional to the electronic stopping power S_e (see Chapter 2). The deduced coefficients Λ_- for proton impact on clean Ag, Al, Au and Cu targets are summarized in Table A2-1. From Figs. A2-2, -3 and -4, it is noticed that γ^- deviates from $\Lambda_- S_e$ at the incident proton energy below 10 keV, where a threshold term for the secondary electron emissions needs to be included [T 1995].

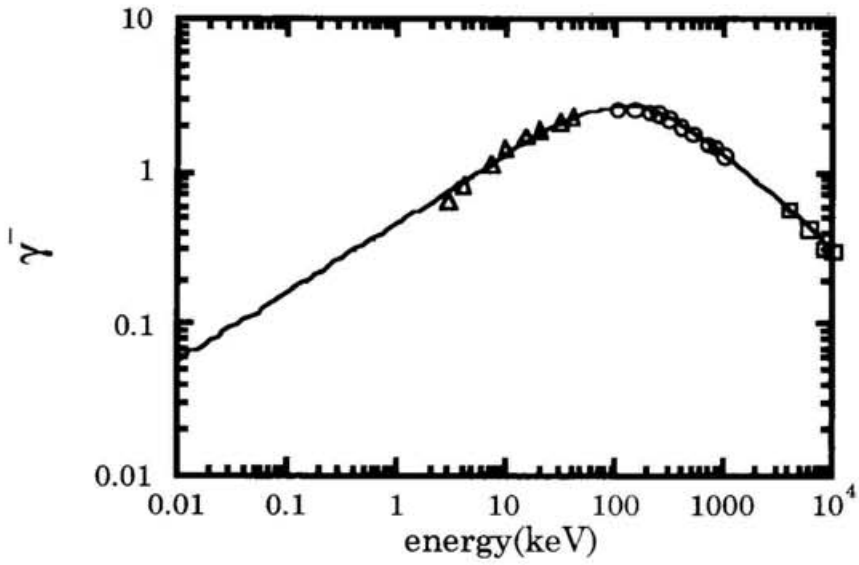

Figure A2-1 The incident energy dependence of γ^- in H^+ impact on clean Ag; ○ Hasselkamp et al., △ Baragiola et al. and □ Koyama et al. The line shows 0.013 S_e.

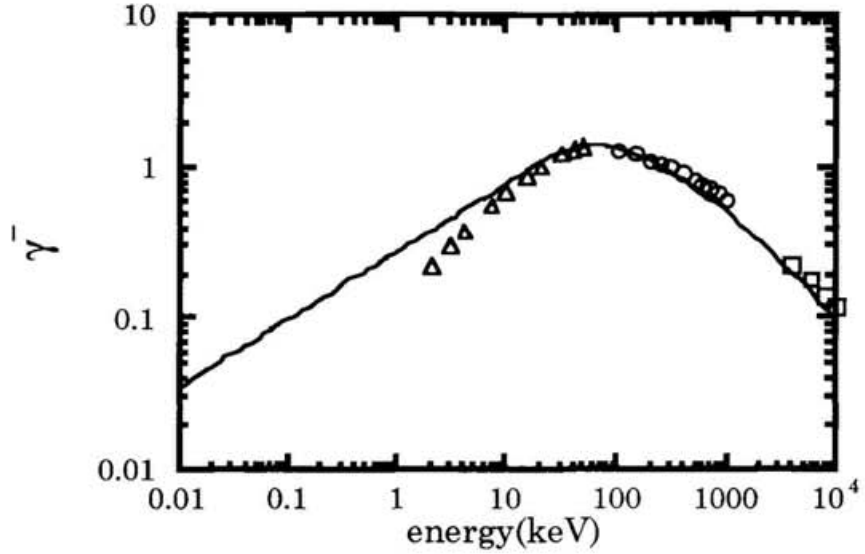

Figure A2-2 The incident energy dependence of γ^- in H^+ impact on clean Al; ○ Hasselkamp et al., △ Baragiola et al. and □ Koyama et al. The line shows 0.011 S_e.

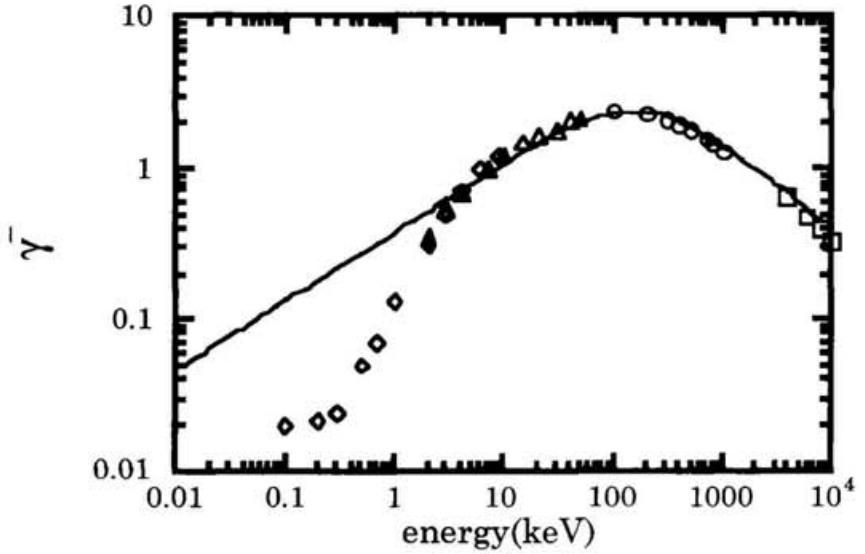

Figure A2-3 The incident energy dependence of γ^- in H^+ impact on clean Au; ○ Hasselkamp et al., △ Baragiola et al., □ Koyama et al. and ◇ Lakits et al. The line shows 0.011 S_e.

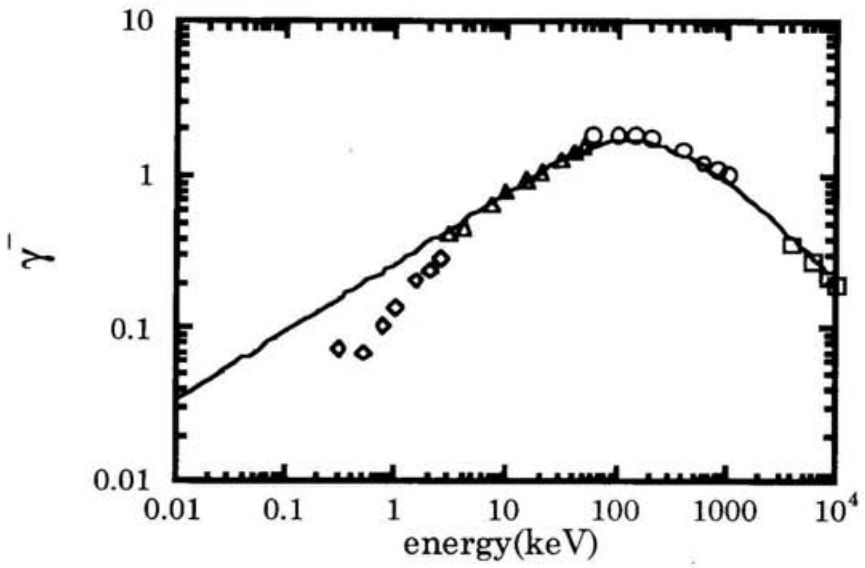

Figure A2-4 The incident energy dependence of γ^- in H^+ impact on clean Cu; ○ Hasselkamp et al., △ Baragiola et al., □ Koyama et al. and ◇ present work. The line shows 0.0086 S_e.

Table A2-1 Proportional coefficients Λ_- (nm/eV) for various metal targets.

	Ag	Al	Au	Cu
H^+	0.013 [1]	0.012 [1]	0.011 [1]	0.0093 [1]
	0.013 [2]	0.0092 [2]	0.011 [2]	0.0086 [2]
	0.012 [3]	0.013 [3]	0.010 [3]	0.0079 [3]
			0.0051 [4]	0.0047 [5]

1) Hasselkamp et al. (1981) 80-1000 keV [HLS 1981]

2) Baragiola et al. (1979) 2-50 keV [BAO 1979]

3) Koyama et al. (1981) 4-12 MeV [KSS 1981]

4) Lakits et al. (1990) 0.1-9 keV [LAH 1990],[LAW 1990]

5) present work 0.3-2.5 keV

References

[BAO 1979] R. A. Baragiola, E. V. Alonso and A. Oliva Florio, Phys. Rev. B 19 (1979) 121

[HLS 1981] D. Hasselkamp, K. G. Lang, A. Scharmann and N. Stiller, Nucl. Instr. Meth. 180 (1981) 349

[KSS 1981] A. Koyama, T. Shikata and H. Sakairi, Jpn. J. Appl. Phys. 20 (1981) 65

[LAH 1990] G. Lakits, F. Aumayr, M. Hein and H. Winter, Phys. Rev. A 42 (1990) 5780

[LAW 1990] G. Lakits, A. Arnau and H. Winter, Phys. Rev. B 42 (1990) 159

[T 1995] E. W. Thomas, Report of International Atomic Energy Agency, INDC (NDS)-322 , (IAEA, Vienna, Feb., 1995)

Appendix 3. The secondary electron emission yields for alkali-halide targets

The deduced coefficients Λ_- for rare gas ion impact on alkali-halides are summarized in Table A3-1. It is noticed that Λ_- for alkali-halide targets are much larger than those for metal targets (see Appendix 2) and strongly depend on the projectile-target combination.

Table A3-1 Proportional coefficients Λ_- (nm/eV) for various alkali-halide targets. Data are taken from ref.[KKR 1975].

	KBr	KCl	NaCl	LiF
He^+	0.36	0.38	0.24	0.17
Ne^+	0.090	0.099	0.091	0.072
Ar^+	0.13	0.13	0.071	0.041
Kr^+	0.12	0.14	0.077	0.046
Xe^+	0.041	0.052	0.030	0.019

Reference

[KKR 1975] W. Köning, K. H. Krebs and S. Rogaschewski, Int. J. Mass Spectrom. Ion Phys. 16 (1975) 243

Appendix 4. Empirical formulas for γ^- under various collisions

In order to estimate the contribution of the backscattered particles to the secondary electron emission, it is necessary to know some related data. Based upon data available, we introduce some important empirical formulas:

1) γ^- from the dirty Cu surfaces under H^0 impact can be given as follows (Kislyakov et al. [KSJ 1975]):

$$\gamma^-_{H0}(E) = 0.608 \times E^{0.693} \qquad E \le 10keV \qquad \text{(A4-1)}$$

$$\gamma^-_{H0}(E) = 0.0384 + 1.78 \times E^{0.222} \qquad E > 10keV \qquad \text{(A4-2)}$$

2) γ^- from the clean Cu surfaces under Ar^+ ion impact is given in the following formulas (Baragiola et al. [BAF 1979] and Hasselkamp et al. [HLS 1981]):

$$\gamma^-_{Ar+}(E) = 0.0428 \times E^{1.21} \qquad E \le 10keV \qquad \text{(A4-3)}$$

$$\gamma^-_{Ar+}(E) = -1.57 + E^{0.376} \qquad E > 10keV \qquad \text{(A4-4)}$$

3) As the contribution of the potential energy to γ^- is small in the present energy range, γ^- is mostly due to the kinetic energy. Therefore, γ^- is expected to be independent of the project charge, namely:

$$\gamma^-_{Ar0}(E) = \gamma^-_{Ar+}(E). \qquad \text{(A4-5)}$$

4) The incident angle dependence of the secondary electron emissions from low energy Ar^0 particles is given as follows (Oda et al. [OKI 1992]):

$$\alpha_{Ar0}(\theta) = -4.62 + \frac{5.62}{\cos(0.471\theta)} \qquad \text{(A4-6)}$$

where θ is given in degree.

5) This angle dependence (A4-6) induced by Ar^0 atom impact is assumed to be also applicable to H^0 atom, and not to depend on the energy of the incident atoms in the present energy range.

In this study, we have used the $\gamma_{H0}(E)$, $\gamma_{Ar0}(E)$ and $\alpha_{Ar0}(\theta)$ derived above from the data for Cu and Ta in order to estimate the secondary electron emissions from the inner surface of the inner cup made of stainless steel under neutral particle bombardment which are given in Tables 6-4 (a)-(e).

References

[BAF 1979] R. A. Baragiola, E. V. Alonso, J. Ferron and A. Oliva-Florio, Surf. Sci. 90 (1979) 240

[HLS 1981] D. Hasselkamp, K. G. Lang, A. Scharmann and N. Stiller, Nucl. Instr. Meth. 180 (1981) 349-356

[KSJ 1975] A. I. Kislyakov, J. Stöckel and K. Jakubka, Sov. Phys. Tech. Phys. 20 (1975) 986

[OKI 1992] K. Oda, T. Kanie, A. Ichimiya, S. Ohtani and H. Tawara, Surf. Sci. 262 (1992) 434-443

Acknowledgments

I would firstly like to acknowledge my supervisor, Professor Hiroyuki Tawara, for his guidance throughout three years of my Ph.D. course and for careful reading of the manuscript.

I would like to thank Dr. Noriaki Matsunami for his extended advises and discussion and also for providing the samples.

Dr. Hiroyasu Iwahara and Dr. Yoshiaki Takai have provided some samples without which the present work could not have been completed.

I wish to thank Mr. Franciszek Krok for his help in the present experiment and his useful discussion, Mr. Satoshi Mashima, Mr. Kenji Matsumoto, Mr. Takeshi Kawamura and Miss Eriko Hatanaka for their help in the present experiment and the calculation by TRIM code and the members of the NICE group for their useful advice and suggestion; Dr. Atsunori Danjo, Dr. Masahiro Kimura, Dr. Atsushi Matsumoto, Dr. Nobuyuki Nakamura, Dr. Shunsuke Ohtani, Dr. Hiroyuki A. Sakaue, Dr. Makoto Sakurai, Dr. Hirofumi Watanabe, Dr. Ichihiro Yamada and Dr. Masuhiro Yoshino.

My thanks are due to Mr. Toshiki Takahashi, Mr. Toshihiro Imai and Mr. Takahiro Kenmotsu for useful discussion.

The financial support for my university life from SHINSYOU-KAI is highly appreciated.

Finally, I would like to express my deep acknowledgments to my parents.